Primaquine and chloroquine nano-sized solid dispersion-loaded dissolving microarray patches for the improved treatment of malaria caused by Plasmodium vivax

Anjani, Q. K., Volpe-Zanutto, F., Hamid, K. A., Sabri, A. H. B., Moreno-Castellano, N., Gaitán, X. A., Calit, J., Bargieri, D. Y., & Donnelly, R. F. (2023). Primaquine and chloroquine nano-sized solid dispersion-loaded dissolving microarray patches for the improved treatment of malaria caused by Plasmodium vivax. *Journal of controlled release : official journal of the Controlled Release Society*, *361*, 385-401. https://doi.org/10.1016/j.jconrel.2023.08.009

Document Version:
Publisher's PDF, also known as Version of record

Queen's University Belfast - Research Portal:
Link to publication record in Queen's University Belfast Research Portal

Primaquine and chloroquine nano-sized solid dispersion-loaded dissolving microarray patches for the improved treatment of malaria caused by *Plasmodium vivax*

Qonita Kurnia Anjani [a,e], Fabiana Volpe-Zanutto [a], Khuriah Abdul Hamid [b],
Akmal Hidayat Bin Sabri [a], Natalia Moreno-Castellano [c], Xiomara A. Gaitán [d], Juliana Calit [d],
Daniel Y. Bargieri [d], Ryan F. Donnelly [a,*]

[a] *School of Pharmacy, Queen's University Belfast, Medical Biology Centre, 97 Lisburn Road, Belfast BT9 7BL, UK*
[b] *Department of Pharmaceutics, Faculty of Pharmacy, Universiti Teknologi MARA Cawangan Selangor, 42300, Puncak Alam, Malaysia*
[c] *Basic Science Department, Faculty of Health, Universidad Industrial de Santander, Bucaramanga 680001, Colombia*
[d] *Department of Parasitology, Institute of Biomedical Sciences, University of São Paulo, São Paulo, Brazil*
[e] *Fakultas Farmasi, Universitas Megarezky, Jl. Antang Raya No. 43, Makassar 90234, Indonesia*

ARTICLE INFO

ABSTRACT

Malaria is a global parasitic infection that leads to substantial illness and death. The most commonly-used drugs for treatment of malaria vivax are primaquine and chloroquine, but they have limitations, such as poor adherence due to frequent oral administration and gastrointestinal side effects. To overcome these limitations, we have developed nano-sized solid dispersion-based dissolving microarray patches (MAPs) for the intradermal delivery of these drugs. *In vitro* testing showed that these systems can deliver to skin and receiver compartment up to ≈60% of the payload for CQ-based dissolving MAPs and a total of ≈42% of drug loading for PQ-based dissolving MAPs. MAPs also displayed acceptable biocompatibility in cell tests. Pharmacokinetic studies in rats showed that dissolving MAPs could deliver sustained plasma levels of both PQ and CQ for over 7 days. Efficacy studies in a murine model for malaria showed that mice treated with PQ-MAPs and CQ-MAPs had reduced parasitaemia by up to 99.2%. This pharmaceutical approach may revolutionise malaria vivax treatment, especially in developing countries where the disease is endemic. The development of these dissolving MAPs may overcome issues associated with current pharmacotherapy and improve patient outcomes.

1. Introduction

Malaria is an infectious disease that affects over 247 million people globally and caused approximately 619,000 deaths in 2021 [1,2]. This mosquito-borne disease arises when single-celled protozoans of the genus *Plasmodium* are transferred into the human systemic circulation during a mosquito bite [3]. Some of the deadliest *Plasmodium* species that cause malaria and also malaria relapse include *Plasmodium falciparum* and *Plasmodium vivax* [4]. *P. falciparum* is known to be the deadliest species to infect humans [1]. However, in regions where both *P. falciparum* and *P. vivax* malaria are present, the prevalence of *P. vivax* malaria has surpassed that of *P. falciparum* [5]. Controlling *P. vivax* is more challenging than *P. falciparum,* because of its capacity to generate

dormant forms in the liver (hypnozoites) [6]. Even after eradicating *P. vivax* schizonts from the blood, infected people may relapse due to the activation of hypnozoites, and as a result, they can spread the infection [4].

The World Health Organization (WHO) recommends the combination of chloroquine (CQ) and primaquine (PQ) as the preferred treatment for malaria infections caused by *P. vivax,* representing the gold standard therapy [1]. CQ acts during the intraerythrocytic stage, where infected erythrocytes containing trophozoite and schizont circulate within the human body and adhere to the vascular endothelium [6,7]. Upon entering the erythrocytes, the deprotonated quinoline ring of CQ accumulates inside the parasite, preventing the toxic heme from crystallising into haemozoin during haemoglobin proteolysis [8]. The

accumulation of heme leads to parasite death *via* autodigestion [8]. CQ has a prolonged effect, with a half-life of 20 to 60 days. The treatment with CQ has potential complications from prolonged use or high doses, including retinopathy, muscle weakness, and toxicity in children [9]. On the other hand, PQ works by generating H_2O_2 that accumulates in the cell and has anti-parasitic activity [10]. PQ acts by eradicating the hepatic stage of *P. vivax*, thus inhibiting the formation of erythrocytic forms that lead to relapses [11]. It also kills gametocytes. PQ is administered once daily for a duration of 2 weeks [12], while for the treatment with CQ is more complicated. Patients are required to take a 620 mg dose of CQ once a day to initiate the regimen, followed by 310 mg after 6–8 h, and 310 mg on the second and third days of treatment [13]. This extended treatment duration may be perceived as burdensome and complex for patients with *P. vivax*, which is necessary to prevent relapses [14]. Therefore, there is a clear need to reformulate these aminoquinolines into a formulation that can be administered easily while providing sustained release over several days. This approach would simplify the treatment regimen, increase adherence, and lead to better therapeutic outcomes.

One formulation approach that could offer these desired advantages are microarray, patches (MAPs). These are arrays of microprojections on a smooth baseplate which, upon application to the skin, will generate channels across the *stratum corneum* [15]. The channels can then be leveraged to deliver a range of therapeutics into and, and in the case of antimalarial therapy, into the skin to form a depot. Subsequently, the drug is released slowly over time [16]. In the current work, we developed, for the first time, dissolving MAPs for the management of malaria vivax. The antimalarial MAPs were then evaluated in terms of mechanical resistance, insertion profile as well as the rate by which the needle layer dissolve within the skin. Additionally, the deposition and permeation profile of PQ and CQ were investigated by delivering them into *ex vivo* porcine skin after the application of MAPs. Furthering this, the delivery profile of PQ and CQ was also evaluated *in vivo* Sprague Dawley rats to evaluate the potential of these system to achieve sustained delivery following a single skin application. The efficacy of the formulations was also evaluated in female mice model for malaria. Overall, the current work demonstrated that dissolving MAPs may provide a patient-friendly strategy to improve the treatment of malaria by offering a simple and sustained delivery approach following a single patch application relative to the more complex and tedious oral based delivery.

2. Materials and methods

2.1. Materials

Primaquine biphosphate (PQ) with a purity of 98% was obtained from Sigma Aldrich (Dorset, UK). Chloroquine diphosphate salt (CQ) with a purity of 98% was acquired from Alfa Aesar (Lancashire, UK). The internal standard, ketoconazole, was purchased from Sigma-Aldrich (St. Louis, MO, USA). Ethyl acetate, the deproteinising agent, was sourced from Fisher Scientific (Loughborough, UK). Soluplus® (a poly(N-vinyl caprolactam)–poly(vinyl acetate)–poly(ethylene glycol) graft copolymer) obtained from BASF (Ludwigshafen, Germany), and PVP 90 kDa (Plasdone™ K-29/32) obtained from Ashland (Kidderminster, UK) were also utilised. Other chemicals and reagents were purchased from Sigma-Aldrich (Dorset, UK).

2.2. Preparation of drug-Soluplus® powder

A series of Soluplus® solutions with concentrations of 0.25%, 0.5%, 1.0%, and 2.0% *w/v* were prepared through serial dilution. Each Soluplus® solution (3 mL) was then individually added to 120 mg of PQ or CQ, and mixed using a SpeedMixer™ DAC 150.1 FVZ-K (German Engineering, Hauschild & Co. KG, Hamm, Germany) at a speed of 3500 rpm for 3 min. Before undergoing lyophilisation, the drug-polymer mixture

obtained was subjected to a temperature-controlled freezer at −80 °C for a period of 3 h. Lyophilisation was carried out using a freeze dryer (Virtis™ Advantage XL-70, SP Scientific, Warminster, PA, USA) for a total duration of 24 h. The process involved a primary drying cycle lasting 13 h, starting at a shelf temperature of −40 °C. This was followed by a secondary drying phase lasting 11 h at a temperature of 25 °C under a vacuum pressure of 50mTorr.

2.3. Characterisation of drug-Soluplus® powder

Size distribution analysis of the formed PQ-Soluplus® and CQ-Soluplus® particles was conducted using Dynamic Light Scattering (NanoBrook Omni® analyzer, Brookhaven, New York, NJ, USA). Prior to analysis, samples were prepared using a similar method with slight modifications [17]. The analysis was performed at a temperature of 25 °C with a 3-min equilibration time before sample analysis. The drug-Soluplus® powders were also visualised using scanning electron microscopy (SEM) with a TM3030 microscope (Hitachi, Krefeld, Germany). To determine the chemical interactions between the drugs and Soluplus®, a Fourier transform infrared (FTIR) spectrometer (Accutrac FT/IR-4100™ Series, Perkin Elmer, USA) was used. The crystallinity of the pure drugs, pure Soluplus®, physical mixture (PM), and drug-Soluplus® powder was evaluated using a differential scanning calorimeter (DSC Q20, TA Instruments, Elstree, Hertfordshire, UK) and an X-ray diffractometer (Rigaku Corporation, Kent, UK).

2.4. Fabrication of dissolving MAPs with drug-Soluplus® tips

A two-step casting approach was used to prepare dissolving MAP containing PQ or CQ, similar to our previously published method [18–20]. Briefly drug-Soluplus® powder (Table 1) and water at a ratio of 33:67 *w/w* were mixed. Once a homogeneous dispersion was obtained, 50 mg of the mixture was introduced into a PDMS mould. The mould contained 600 pyramidal needles, each with a height of 750 μm, and was distributed over a 0.76 cm^2 area. The PDMS moulds were transferred into an enclosed chamber and subjected to a positive pressure of 4 bar for 5 min. Afterwards, the formulations were taken out of the chamber and any excess mixture were removed before allowing the needle layer to dry for 30 mins. Once the system was dried, a PDMS ring was secured around the mould using 40% of *w/w* PVA (9–10 kDa) as this will assist in the fabrication of the backing layer. Then, 850 μL of backing layer mixture consisting of 30% w/w of PVP (90 kDa) with the addition of 1.5% of w/w glycerol was added on top of the needle layer. The system was then centrifuged at 3500 RPM for 15 mins before being left to air dry. Once dry, the MAPs were demoulded and dried for another 12 h in a thermostatically controlled oven prior to further experimentation.

2.5. Study of mechanical strength and insertion into ex vivo skin

The structure and morphology of the each MAP were examined using a digital microscope (Leica EZ4 D, Leica Microsystems, Milton Keynes, UK). The compression resistance of the needles was assessed using a TA-TX2 Texture Analyzer (TA) from Stable Microsystems in Haslemere, UK), following the parameters described in previous studies [21,22]. The changes in needle height were estimated by subjecting them to a compressive force of 32 N, and Eq. (1) was used for measurement.

Table 1
Formulation for PQ and CQ loaded dissolving MAP preparation.

MAP formulation	Ratio of the drug to Soluplus®
F1	8:1
F2	4:1
F3	2:1
F4	1:1

$$MAPs\ height\ reduction\ (\%) = \frac{H_{initial} - H_{after}}{H_{initial}} \times 100\% \qquad (1)$$

where $H_{initial}$ represents the initial height of the needle, and H_{after} denotes the height of the needle after compression.

The insertion characteristics of the MAPs into Parafilm® M (as a validated skin model) and *ex vivo* neonatal porcine skin were examined using an EX-101 optical coherence tomography (OCT) microscope (Michelson Diagnostics Ltd., Kent, UK), following the methodology described in a previous study [23]. OCT images were captured to visualise the depth of needle insertion, and ImageJ® software (National Institutes of Health, Bethesda, MD, USA) was utilised to calculate the precise insertion depth.

2.6. Quantification of drug loaded in the MAPs

The drug content in the MAPs was determined by placing the formulation in a glass vial and dissolving it in 4 mL of deionised water. To enhance the dissolution process, the patch was sonicated for 30 min using an Ultrawave ultrasonic steriliser (U100, Ultrawave, Ltd., Cardiff, UK) set at an ultrasonic power of 35 W. The resulting mixture was diluted twofold with methanol and subjected to another 30 min of sonication. Afterward, the final mixture underwent centrifugation at 14,500 rpm for 15 min before analysis using HPLC.

2.7. In situ dissolution study of MAPs

An *in situ* skin dissolution study was conducted to determine the time required for the MAPs to dissolve in neonatal porcine skin. Full-thickness neonatal porcine skin tissue was immersed in PBS (pH 7.4) at 37 °C for 30 min to reach equilibrium. The surface of the skin was then gently dried using a paper towel, and the MAPs were manually inserted into the skin using thumb pressure for a duration of 30 s. To prevent the MAPs from dislodging, a cylindrical stainless steel weight weighing approximately 15 g was placed on top of each MAP. The samples were then placed in an oven set at 37 °C and analysed at specific time intervals. The analysis involved carefully peeling off the samples from the skin and examining them under a digital microscope.

2.8. Dermatokinetic study

Dermatokinetic studies were conducted using excised full-thickness neonatal porcine skin to investigate the delivery of PQ and CQ from MAPs, following a previously published method. [17,24,25]. Briefly, the excised skin was attached to the donor component of the apparatus using cyanoacrylate adhesive. The receiver fluid, consisting of degassed PBS (pH 7.4) at 37 °C, was stirred at a constant rate in a thermostatically regulated water bath. Each MAP was applied to the skin under pressure for 30 s and then clamped to the receiver compartment. To prevent evaporation, the sampling arm and donor component were sealed using Parafilm® M. At specified time intervals, the Franz cells were disassembled, and 200 μL of the receiver solution was collected and analysed using HPLC. The skin samples were homogenised in deionised water, followed by the addition of acetonitrile. After centrifugation, the supernatant was filtered before HPLC analysis.

The analysis of PQ and CQ samples from *in vitro* studies was conducted using reversed-phase high-performance liquid chromatography (HPLC) on an Agilent Technologies 1220 Infinity compacted LC series system (Agilent Technologies UK Ltd., Stockport, UK) equipped with a UV detector. Chromatographic separation was achieved using an XSelect CSH C$_{18}$ column with a 3.0 mm internal diameter, 150 mm length, 3.5 μm particle size, and a pore size of 130 Å (Waters, Dublin, Ireland). A VanGuard® cartridge (3.9 mm internal diameter, 5 mm length) with similar chemistry to the main column was placed before the column. The sample was eluted with a mobile phase consisting of 0.1% *v*/v trifluoroacetic acid (A) and acetonitrile (B) (refer to Table 2 for details) at a

Table 2
HPLC parameter for *in vitro* analysis of PQ and CQ.

Compound	Ratio of mobile phase (A:B) (%*v*/v)	Wavelength (nm)	Running time (min)
PQ	75:25	254	7
CQ	65:35	254	5

flow rate of 0.6 mL/min. The HPLC analysis was performed at 30 °C, and a 10 μL injection volume was used.

2.9. Biocompatibility study

The biocompatibility of MAPs was evaluated using three assays, namely 3-(4,5-dimethylthiazol-2-yl)-2,5-diphenyl tetrazolium bromide (MTT), LIVE/DEAD™, and cell proliferation assays (pico-green). The evaluation was performed using a similar method as previously published [17,25]. Briefly, fibroblast-3T3L1 cells were cultured with DMEM culture medium (DMEM-F12-GlutaMAX-I, Gibco, New York, NY, USA) on MAP formulations for 72 h. The MTT assay was performed by adding MTT solution to the cells, followed by the addition of DMSO to dissolve the formazan crystals. The optical absorbance of the solution was measured at 570 nm using a microplate reader (Biotek, Winooski, VT, USA). Cell viability and proliferation assays were conducted to evaluate the effects of MAP formulations on Fibroblast-3T3L1 cells. For cell viability, live/dead staining was performed using calcein AM and ethidium homodimer-1. The stained cells were observed under a fluorescence microscope to determine the presence of live and dead cells. To assess cell proliferation, a Quant-iT™ PicoGreen® dsDNA Reagent and Kits were used.

2.10. Pharmacokinetic studies

Six male Sprague Dawley rats weighing 300–350 g were obtained from the Laboratory Animal Facility and Management (LAFAM), Universiti Teknologi MARA (UiTM) Puncak Alam, Selangor, Malaysia. The animal experiments were conducted following the guidelines of the Committee on Animal Research & Ethics (CARE) of the Faculty of Pharmacy, UiTM. The rats were sedated using an intraperitoneal injection (IP) of Zoletil®50 (0.1 mL/100 g rat weight) and their back fur was shaved with electric clippers. After complete fur removal, two dissolving MAPs were applied to the back of each rat and secured in place with Microfoam™ surgical tape (3 M, Bracknell, UK), and then Kinesiology™ tape (Proworks, Stockton, UK). For the oral treatment group, the rats were fasted overnight and then administered 30 mg/kg of PQ or CQ *via* oral gavage. Blood samples were taken from the tail vein at predetermined time intervals (0, 2, 4, 8, 12, 24, 48, 72, and 168 h) using a heparinised syringe with needle and the plasma was frozen at −80 °C until further analysis. In order to elucidate the hepatoxicity of the formulations, the liver of the rats was collected post-mortem and fixated using 10% neutral buffered formalin in a capped and leak-proof container. The livers were sectioned, stained with haematoxylin and eosin (H&E), and mounted with a coverslip using optical grade glue.

A rapid and precise method for measuring PQ and CQ in rat plasma was established using UHPLC-MS/MS technology. The UHPLC-MS/MS system used was composed of an Agilent 1200 infinity UHPLC system with an Agilent 6460 triple-quadrupole mass spectrometer (Santa Clara, CA, USA). Chromatographic separation was performed at 40 °C using an Zorbax SB-C18 Rapid Resolution HT (2.1 m × 50 mm, 1.8 μm) with (A) 0.1% formic acid in water and (B) methanol. The gradient elution program was 0.00–3.00 min, 5–95%; 3.00–4.00 min, 5–95%; and 4.00–4.10 min, 60–40%. The sample injection volume was 2 μL and the flow rate was set at 0.250 mL/min. A calibration curve was prepared with 200 μL of blank rat plasma spiked with both standards at different concentrations. For plasma extraction, 100 μL of the sample was mixed with 10 μL of internal standard (ketoconazole) and 1 mL of ethyl acetate

to precipitate the protein. After centrifugation, 950 μL of the supernatant was transferred to a new microcentrifuge tube and dried using a benchtop centrifugal evaporator. The dried sample was then reconstituted with 50 μL of 50% methanol in ddH$_2$O with 0.1% added, followed by vortex mixing and centrifugation. The resulting supernatant was injected into the LC/MS-QQQ system for analysis.

2.11. In vivo antimalarial activity in plasmodium berghei-infected mice

The formulation efficacy experiment was conducted at the animal facility of the Institute of Biomedical Sciences at the Sao Paulo University (USP), Sao Paulo, SP, Brazil. The parasitemia inhibition of the MAPs was evaluated over a period of 7 days using female mice (C57BL/6, 4 weeks old, 20 ± 3 g) infected with *Plasmodium berghei* under the registration number 9215030119 obtained from the Ethics Committee on the Use of Animals (CEUA). Mice were acclimatised in pathogen-free animal care facility in polypropylene cages. The animals were split into four cohorts ($n = 7$): 1) Control group: blank MAP (without drug). 2) PQ-MAP (1.4 mg); 3) CQ-MAP (3.4 mg); and 4) Combination of PQ-MAP (1.4 mg) and CQ-MAP (3.4 mg). On day 0, the groups were shaved and infected *via* intraperitoneal injection with 1×10^5 *P. berghei* ANKA HSP70-GFP-infected erythrocytes. After 24 h, treatment began by MAP application which was removed only on day 7 following a modified Peter's 4 day suppressive test [26]. Parasitemia was evaluated daily by analysing the whole blood (1 drop of blood +300 μL of PBS) by flow cytometry (488 nm – laser; 540 nm - emission filters) (FACSCalibur) until the end of the treatment (7 days). Parasitemia inhibition was determined in percentage relative to the blank MAP group (without drug or untreated group) [27].

2.12. Stability study of MAPs

The stability of MAPs was evaluated in terms of drug content and height reduction of the needles over time after storing samples at 25 °C/RH 65% and 40 °C/RH 75% were analysed at each predetermined time point (7, 14, 30, 60 and 90 days). The MAPs were stored at in designated boxes during the period of stability study, as previously reported [28].

2.13. Statistical analysis

Statistical analysis of the data was performed using GraphPad Prism® version 8.0 (GraphPad Software, San Diego, California, USA). The data is presented as means ± standard deviation (SD), unless specified otherwise. One-way analysis of variance (ANOVA) was conducted to compare multiple groups, while Student's *t*-test was used for comparisons between two groups. A significance level of $p < 0.05$ was considered statistically significant for all analyses.

3. Results and discussion

3.1. Characterisation of PQ-Soluplus® and CQ-Soluplus® powder

Prior to fabricating the MAPs, we developed and characersed a nano-sized solid dispersion powder of PQ and CQ mixed with Soluplus®. This step was crucial as the nano-sized solid dispersion of these drugs would form the needle layer of the dissolving MAP during manufacturing. To achieve this, we casted the aqueous mixture of nano-sized solid dispersion into the MAP mould to fill the cavity. As the mixture dried, it resulted in the formation of needle-shaped solid dispersions of the drugs. These needles could be easily removed from the moulds, and then the aqueous polymer was cast as the second layer or baseplate, which attached to the needle layer to form the final patch.

In this study, we utilised Soluplus® (Poly(vinyl caprolactam–polyvinyl acetate–polyethylene glycol) graft copolymer) as both the polymeric carrier and surfactant to create the nano-sized solid dispersion. This approach aimed to improve the solubility and permeability of CQ and PQ, consequently enhancing the drug loading in the patch. Furthermore, incorporating the nano-sized solid dispersion of PQ and CQ as the tips aimed to maximise the penetration ability when combined with MAPs, thereby facilitating the intradermal deposition of the drugs.

It can be seen from Fig. 1 (A,B) that the addition of Soluplus® during the formation of drug solid dispersion had a marginal effect on the overall drug particle size for both PQ and CQ. However, it is worth noting that, with increasing Soluplus® concentration, 0.25–2.0%, there was a decrease in the polydispersity index (PDI) of the solid dispersion powder from ≈0.15 to ≈0.05 for PQ and from ≈0.10 to ≈0.05 for CQ. PDI is typically used in colloidal science as a means of measuring the size dispersity of nanoparticulate systems and powders [29]. It is typically reported that a system that displays a PDI of <0.1 is deemed to be highly monodisperse, while those exhibiting values ranging between 0.1 and 0.4 are deemed to be moderately disperse [30]. Based on the PDI data shown, it can be seen that increasing the concentration of the polymeric solubiliser, Soluplus®, causes the solid dispersion system to shift from being moderately dispersed to becoming highly monodisperse. We have previously reported that the incorporation of Soluplus® during the manufacture of nanosuspension and solid dispersion has resulted in the formation of a highly monodisperse colloid and solid dispersion [31,32]. It is also worth noting that freeze drying (FD) process did not have a significant impact on the overall drug-polymer particle size and PDI for PQ. The same could also be seen for CQ, although at higher Soluplus® concentrations (1.0–2.0% *w/v*), we noticed a significant decrease ($p <$ 0.05) in the overall drug-polymer particle size following lyophilisation.

In order to elucidate further the impact of incorporating Soluplus® in the preparation of nano-sized solid dispersions for PQ and CQ, several solid-state characterisation techniques were conducted on the drug-polymer powders as well as the pure reference materials. Fig. 2(A) displays the FTIR analysis, which showed that PQ and CQ spectra exhibited similar peaks to the pure drugs, indicating that the chemical structure of the drugs was not affected by the formation of drug-Soluplus® solid dispersion. Furthering this, the DSC and powder XRD were also conducted in order to further gauge the solid state of drug-polymer powder. The DSC thermogram of PQ and CQ is displayed Fig. 2(B). The endotherm of both PQ and CQ remained unchanged when physically mixed with Soluplus®. However, when the drugs formed nano-sized solid dispersion with Soluplus® following lyophilisation, the characteristic endotherms of both PQ and CQ were affected, leading to the formation of an amorphous and ssemi-crystalline solid dispersion of CQ and PQ, respectively. With regards to PQ, the endotherm of the drug at 206 °C became shallower with increasing Soluplus® concentration while in the case of CQ, the endotherm of the drug was completely absent with all Soluplus® concentrations, once the solid dispersion powder was formed. When these data were viewed in tandem with XRD diffractograms shown in Fig. 2(C), the addition of Soluplus® followed by lyophilisation led to the formation of an amorphous solid dispersion of both CQ and PQ.

SEM imaging was used to examine the physical and structural properties of drug-polymer powders at the micron scale (Fig. 3). SEM analysis of pure PQ and CQ drugs showed irregular crystalline particles, while Soluplus® appeared as spherical particles with porous structures. Physical mixtures of PQ and CQ with Soluplus® showed no incorporation between the two components before lyophilisation. After lyophilisation, drug crystals and Soluplus® spheres were no longer present, making it difficult to distinguish between the two components. When Soluplus® concentration increased from 0.25 to 2.00% *w/w*, resulting powders were more uniform and porous, indicating successful incorporation of drug particles with Soluplus®. SEM observation, combined with DSC and XRD data (Fig. 2), showed that drug-polymer powder between Soluplus® and the API formed an amorphous solid dispersion system.
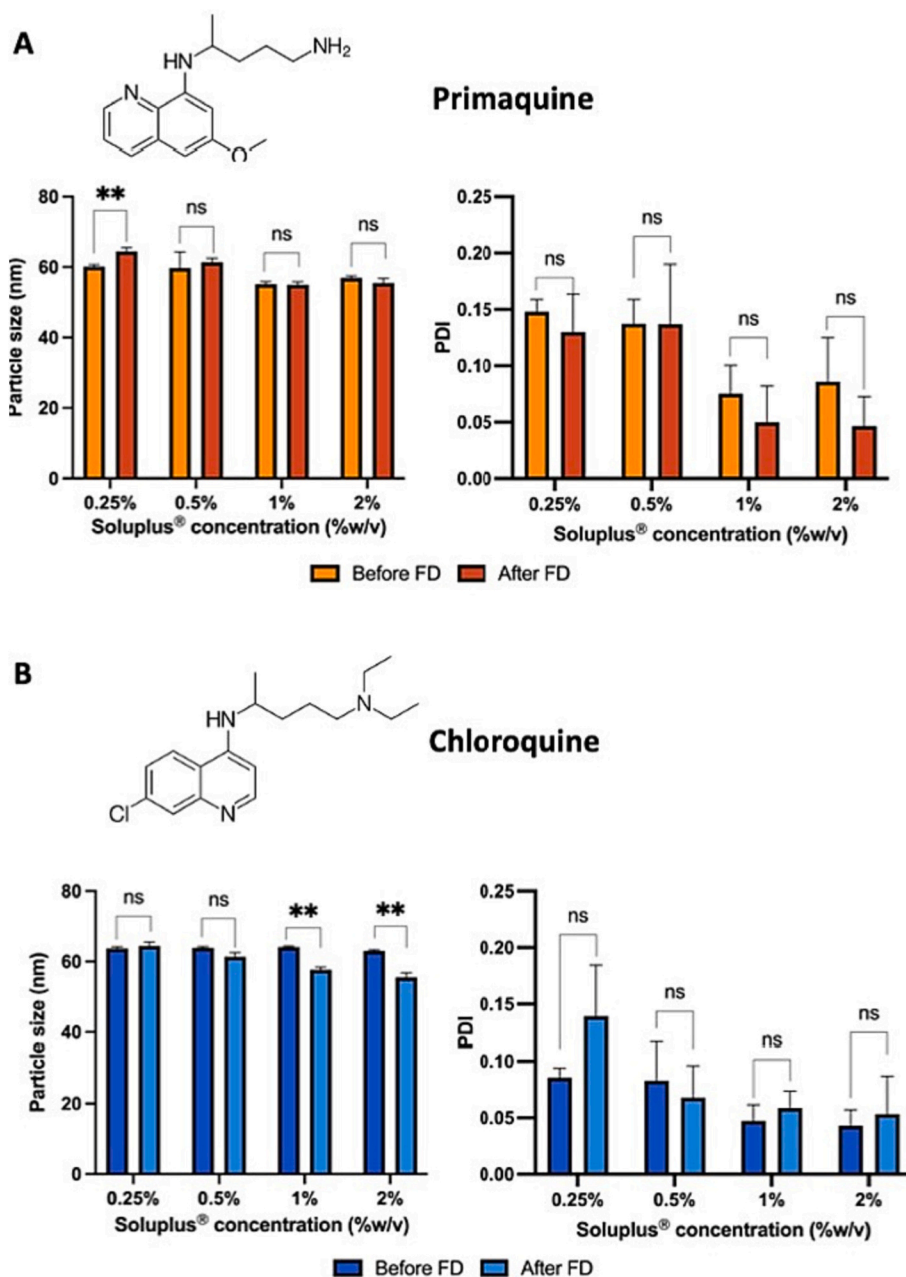
Fig. 1. The particle size and polydispersity index (PDI) of the (A) PQ-Soluplus® powder and (B) CQ-Soluplus® powder were measured before and after freeze drying (FD) process (means + SD, $n = 3$).

3.2. Fabrication of dissolving MAPs with drug-Soluplus® tips

PQ loaded dissolving MAPs appeared as patches with orange tips, while CQ loaded dissolving MAPs appeared white and opaque post-fabrication, as shown in Fig. 4. The orange colour of the PQ loaded dissolving MAPs was due to the intrinsic colour of the drug, which is an orange-to-brown powder. The majority of the drug was localised within the tip of the MAP, as can be seen in Fig. 4. High drug:polymer ratios (8:1 to 2:1) for PQF1-PQF3 resulted in poorly formed PQ-loaded dissolving MAP patches, with chipped MAP and poorly formed needle tips visible in optical microscopy and SEM images. The highest drug:polymer ratio (PQ-F1) showed completely broken needle tips with porous structures along the needle length. This has observation has been reported for dissolving MAP with high drug solid content in the needle tip [33,34]. This issue was resolved by increasing the Soluplus® content in the needle layer, which improved MAP morphology. The higher Soluplus®

content in the needle layer helped trap residual moisture in the needle as an external plasticiser, enabling effective demoulding post-drying [35]. The presence of higher polymer content in the needle layer also functioned as a binder, helping interlock drug particles within the needle layer and reducing the formation of highly porous needle structures post-drying [35]. This phenomenon may be highly dependent on the payload incorporated in the dissolving MAP, as it was not encountered in the case of CQ.

After visual and microscopic characterisation of the MAPs, we evaluated the drug loading within the patch tips, as presented in Fig. 5. It was observed that as the drug to polymer ratio decreased from 8:1 to 1:1 in all formulations, the drug loading for both PQ and CQ loaded dissolving MAPs also decreased. At the highest drug to polymer ratio of 8:1, we were able to achieve a drug loading of 2.6 mg per patch for PQ and 3.4 mg per patch for CQ.
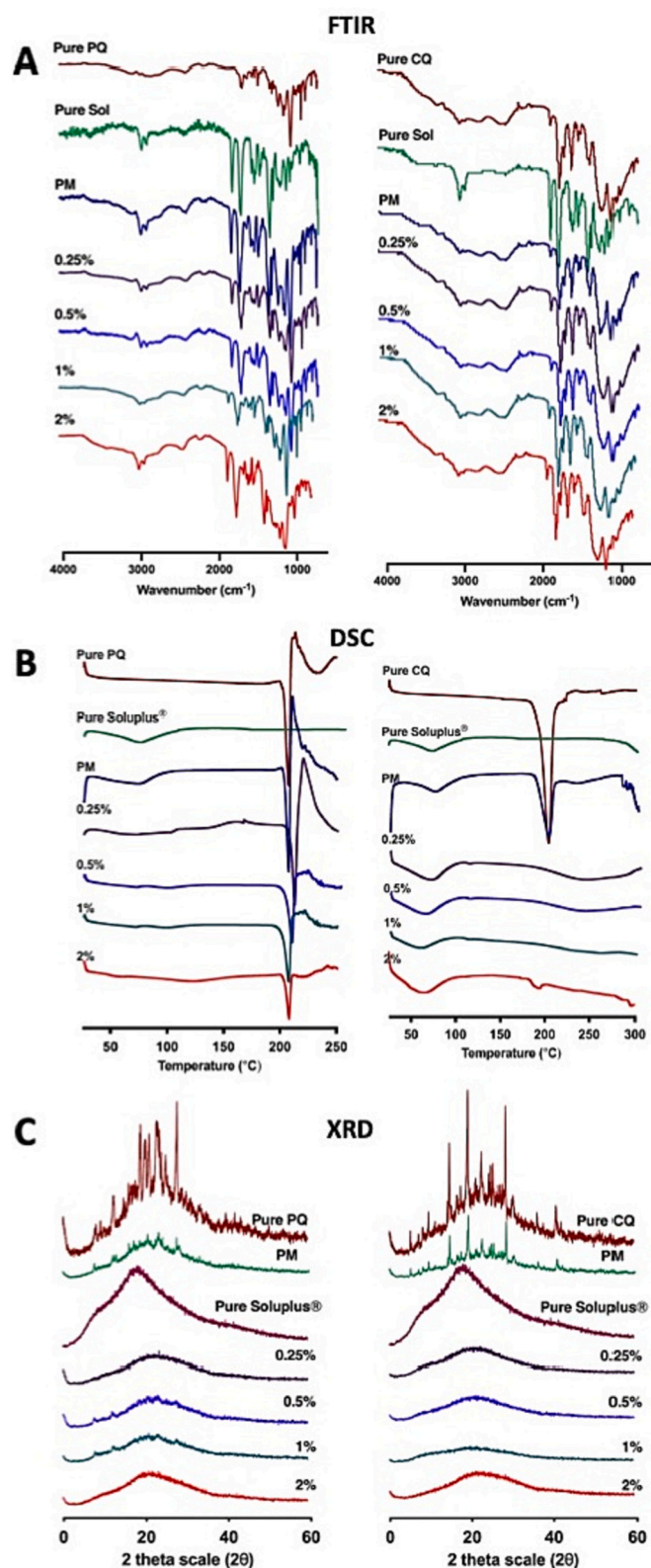
Fig. 2. (A) FTIR spectra (B) DSC thermogram and (C) XRD diffractogram of PQ-Soluplus® powder and CQ-Soluplus® powder at different concentration of Soluplus®, 0.25%, 0.5%, 1%, 2% compared to pure drug, pure Soluplus® and physical mixture (PM).

3.3. MAP characterisation studies

Upon fabricating the drug loaded dissolving MAPs, the patches were then subjected to a series of characterisation studies which are commonly conducted in most MAP-based research as a means to confirm that the developed patches have the ability to pierce and dissolve in the skin to enable the release of the payload [32,36]. First, the series of dissolving MAPs for PQ and CQ were subjected to a compression test by which per 0.76 cm^2 patch was subjected to an axial force of 32 N which is comparable to thumb pressure. This test was conducted in order to ascertain if the fabricated MAPs will be able to resist the compressive force, with minimal height reduction, during skin application. It can be seen from Fig. 6 that the drug loaded patches exhibit an initial needle length of ≈620 μm which upon compression causes the height to be reduced by ≈6.0%. This is the typical % of height reduction typically reported for dissolving MAPs which possess sufficient mechanical properties for skin insertion [31,32,34].

Furthermore, insertion studies using either the skin simulant, Parafilm®M or *ex vivo* neonatal porcine skin, were conducted to evaluate the insertion properties of the developed series of MAPs. Examples of representative OCT images of the MAPs being inserted into Parafilm®M or *ex vivo* neonatal porcine skin are shown in Fig. 6 (C,D). As shown in Fig. 6 (E), all the PQ-loaded MAP formulations were able to insert with a 100% efficiency into the first layer of the Parafilm®M stack, as evidenced by the absence of any error bars. Moreover, all the PQ-loaded MAP formulations were able to insert down to the third layer of Parafilm®M. Monitoring the insertion *via* OCT, it was shown that all the MAPs resulted in an insertion depth of 300–350 μm, as displayed in Fig. 6 (F). In terms of the CQ-loaded MAPs, all the formulations exhibited a similar insertion profile to the PQ-loaded dissolving MAPs. However, with regards to Parafilm®M insertion, it was observed that the CQ-loaded MAPs displayed a significantly ($p < 0.05$) deeper insertion relative to the PQ-loaded MAPs. When both series of formulations were evaluated using *ex vivo* neonatal porcine skin, we observed several differences in the MAPs' insertion profiles into Parafilm®M. Firstly, all the patches displayed a deeper insertion depth relative to the porcine skin, relative to the insertion profile into the stacks of Parafilm®M, which has been previously observed and reported [31,32]. The deeper insertion depth for both PQ and CQ-loaded MAPs into *ex vivo* skin relative to Parafilm®M may be due to the presence of dermal interstitial fluid. This naturally occurring fluid in the skin will be encountered by the surface of dissolving MAPs, thus, providing some lubrication that mitigates frictional resistance during the penetration of the MAPs into the skin relative to Parafilm®M. Based on the *ex vivo* skin insertion depth, it can be seen that approximately 70–80% of the needle length was successfully inserted into the skin, suggesting that the drug-loaded tip would be successfully embedded into the skin upon application.

Following the insertion studies, we proceeded to evaluate the dissolution profile of a series of PQ and CQ-loaded dissolving MAPs following application to the skin. Fig. 7 shows that for PQ-loaded dissolving MAPs, formulations F1-F3 displayed minimal dissolution within 15 min of skin insertion. However, after 30 min of skin application, the majority of the needle length had dissolved and deposited into the skin for formulations F1-F3. In contrast, PQ-F4 displayed complete needle dissolution following 15 min of skin application. With regards to CQ-loaded dissolving MAPs, we observed that F1 showed the most rapid dissolution, with almost all the needle tips displaying complete dissolution within 15 min of skin application. On the other hand, formulations F2-F4 for CQ loaded dissolving MAPs displayed mostly needle tip dissolution within the first 15 min of skin insertion. However, when these formulations were inserted for up to 30 min, we observed complete dissolution of the entire needle lengths. Guided by the skin dissolution data in tandem with the drug loading of these formulations, formulation F1 for CQ-loaded dissolving MAPs and F4 for PQ-loaded dissolving MAPs were selected for further evaluation *in vitro* before proceeding to an *in vivo* pharmacokinetic and efficacy study.
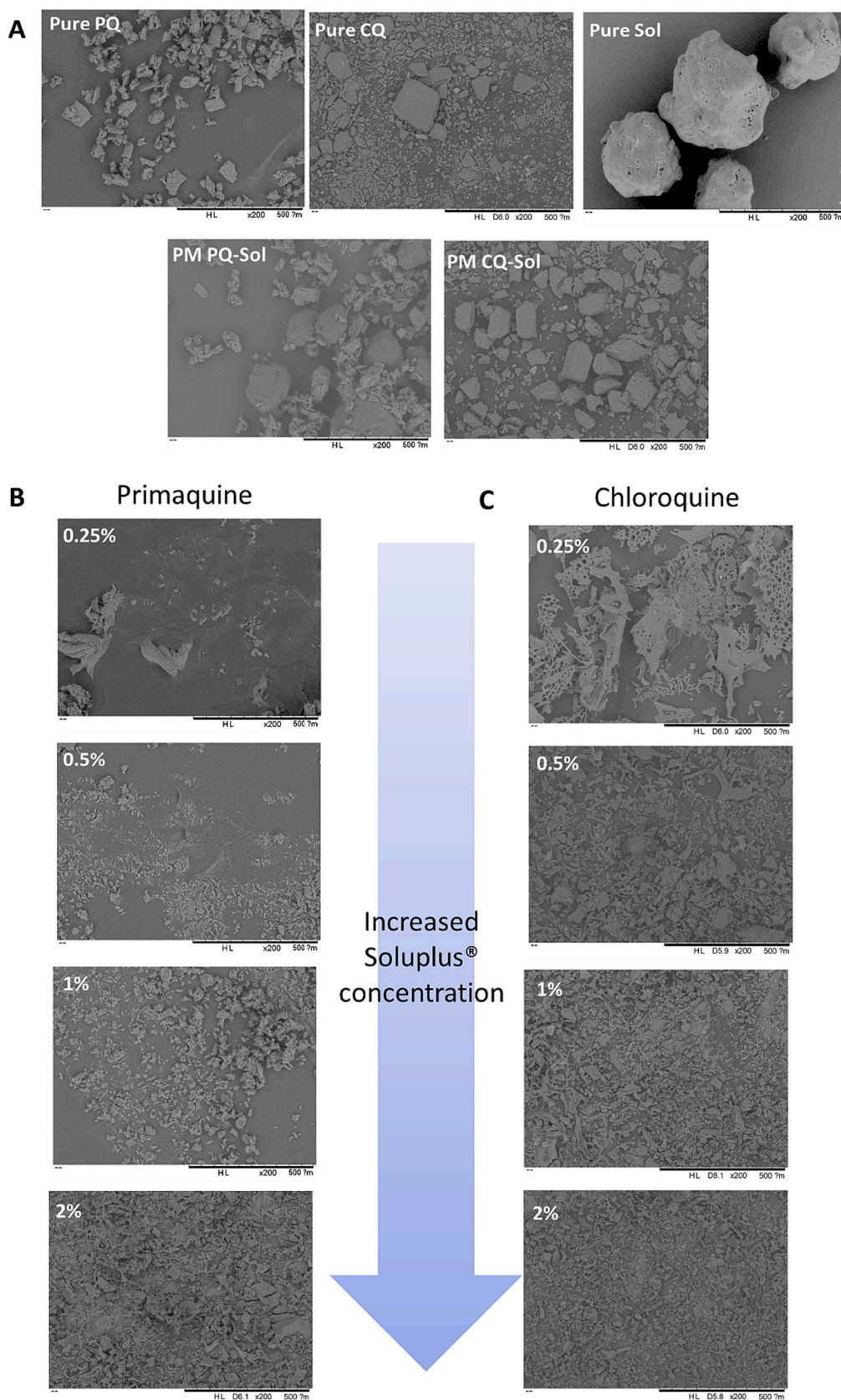
Fig. 3. SEM images (A) Pure drug and polymer powder along with different physical mixture (B) PQ-Soluplus® powder (C) CQ-Soluplus® powder at different concentration of Soluplus®, 0.25%, 0.5%, 1%, 2%.
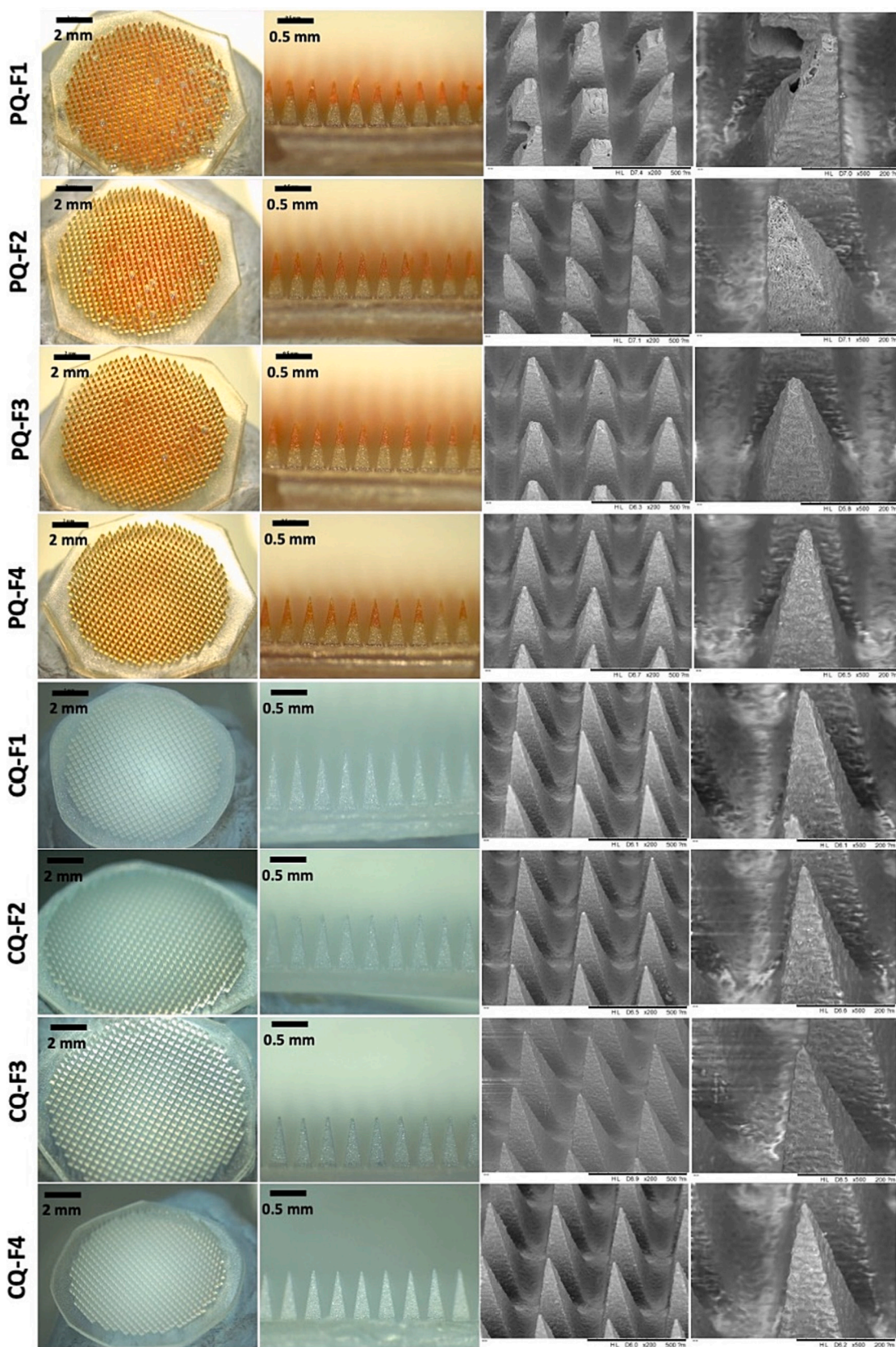
Fig. 4. Optical microscopy and SEM images of PQ and CQ solid dispersion MAPs with different Soluplus® concentration.
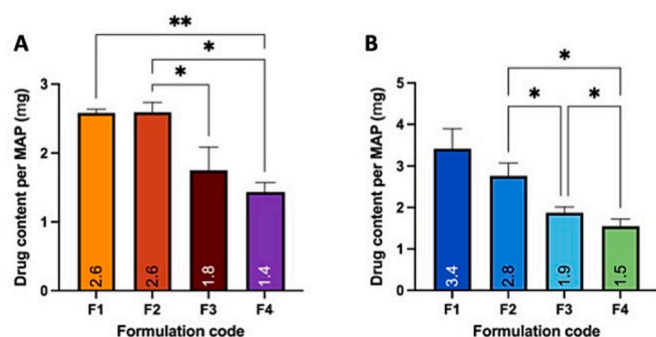
Fig. 5. Drug content of (A) PQ and (B) CQ loaded dissolving MAPs (means + SD., $n = 6$).

3.4. Dermatokinetic study

After conducting a skin dissolution study, we conducted an *ex vivo* dermatokinetic study using a Franz cell setup to evaluate the delivery profile of PQ and CQ into and across the skin, as illustrated in Fig. 8(A). The delivery of PQ and CQ across the skin follows a series of events as illustrated in Fig. 8(B), which begins with the insertion of the microneedle layer into the skin, resulting in the formation of a drug polymer depot within the skin. Over time, this drug polymer depot slowly dissolves, resulting in the slow release of the drug into the skin, which ultimately diffuses into the receptor compartment.

Regarding skin deposition, as shown in Fig. 8(C,D), we observed an increase in the concentration of PQ delivered into the skin within the first 6 h, reaching a skin Cmax of 200 µg/cm^2 before plateauing at 100 µg/cm^2 for the remaining duration of the permeation study. CQ exhibited a similar trend to PQ, but the MAP managed to achieve a more rapid skin Cmax of 800 µg/cm^2 within the 3 h of the permeation study before plateauing at 400 µg/cm^2 for the later time point of the permeation study. This higher skin deposition is attributed to the higher drug loading of CQ (3.4 mg per patch) compared to PQ (1.4 mg per patch), resulting in a greater amount of drug being deposited in the skin over time.

Regarding the delivery of antimalarial drugs across the skin, we can see that for PQ, the amount of drug delivered into the receiver compartment increases within the first 6 h before plateauing at ≈500 µg for the remainder of the permeation study. In contrast, the CQ-loaded dissolving MAP exhibited a steady increase in the amount of drug delivered through the duration of the permeation study, reaching a maximum of 1800 µg at the 24-h time point. Regarding the amount of drug delivered, we can see that for the CQ-loaded dissolving MAPs, a total of 2 mg of CQ was successfully delivered from the formulation within 24 h. It is important to note that both PQ and CQ exhibit different drug deposition and release profiles due to the varying amounts loaded into one patch for each drug. As previously discussed, the higher amount of CQ deposited into the skin leads to the formation of a secondary reservoir, resulting in a slower release of the drug into deeper layers of the skin and eventually reaching the systemic circulation, represented by the receiver compartment. From a delivery efficiency perspective, this equates to a delivery efficiency of ≈60%. On the other hand, we were able to deliver up to 0.6 mg of PQ *via* dissolving MAPs, resulting in a delivery efficiency of ≈42%.

From a formulation perspective, the concept of using MAPs for the delivery of antimalarial drugs was first conceptualized in 2017 by PATH, a global non-profit organization with the aim of improving public health [37]. In this initial framework, the PATH team led by McGray et al. [37] assessed the technical and feasibility of MAPs for the intradermal delivery of the antimalarial drug primaquine to treat *P. vivax* infection. Although lacking in any empirical data, this initial feasibility laid a key target product profile which ought to be incorporated in the design of MAPs for the management of malaria. One of the critical attributes identified is the ability of MAPs to deliver the antimalarial drug in a sustained and uniform fashion following a single patch application. Nevertheless, it was not until 2021 that Zanutto et al. [38] published the first-ever paper on the use of MAPs for the delivery of antimalarial drugs. In this work, Zanutto and co-workers utilised dissolving MAPs to deliver the antimalarial drugs artemether and lumefantrine into and across the skin [38]. In contrast to the current work, the needle layer of the formulation was loaded with a nanosuspension of either artemether or lumefantrine. When evaluated *ex vivo* using a Franz cell setup, the researchers found that the dissolving MAPs were able to deliver up to 1.2 mg of artemether into the skin, with a delivery efficiency of 75%, and 0.2 mg of lumefantrine, with a delivery efficiency of 15%, into and across the skin. When this data is viewed in combination with the *ex vivo* dermatokinetic data obtained in the current work, it can be seen that the utilisation of dissolving MAPs offers an elegant strategy to deliver the drug across the skin. This is of great advantage as it is frequently reported that the delivery of antimalarial drugs *via* the oral route, although convenient, does suffer some significant drawbacks such as gastrointestinal side effects [39].

3.5. Biocompatibility studies

To investigate the effect of MAPs on the biocompatibility of fibroblasts, we evaluated the viability, morphology, and proliferation of cells treated with blank-MAP, PQ-MAP, CQ-MAP, and control cells using an MTT assay and live and dead staining. As shown in Fig. 9(A), PQ-MAP significantly increased cell viability compared to control cells ($p <$ 0.05) and blank-MAP ($p < 0.05$). However, a significant increase in CQ-MAP was found compared to control cells, MAP-blank, and PQ-MAP ($p < 0.05$). Similarly, live and dead staining showed a change in cell morphology after MAP treatment and an evident increase in cell number after PQ-MAP and CQ-MAP treatment, as shown in Fig. 9(B). In addition, the proliferation assay (Fig. 9(C)) showed a significant increase in fibroblast proliferation with PQ-MAP compared to control cells ($p <$ 0.05), blank-MAP and CQ-MAP ($p < 0.05$). CQ-MAP also showed a significant increase in fibroblast proliferation compared to control cells and blank-MAP ($p < 0.05$), suggesting that cells in PQ-MAP and CQ-MAP formulations were more proliferative than those in the other experimental groups. However, despite the high proliferation of CQ and PQ, it was demonstrated that the PQ-MAP and CQ-MAP formulations utilised in this study are biocompatible with fibroblast cells and can be viably employed on the skin.

Previous studies have shown that blank-MAP, which was not loaded with any drugs, has good biocompatibility and does not affect the viability and proliferation of fibroblast cells in a manner similar to control cells [17,25]. Our results also demonstrate good biocompatibility of MAPs-contained CQ, with CQ-MAP even increasing cell proliferation. These findings are consistent with previous studies that have described the decelerating effect of CQ on inflammation in burn wounds and its potential to promote repair and healing of burn wounds, mainly mediated by its effect on autophagy inhibition and the Wnt/β-catenin signalling pathways in fibroblast cells in animal models [40]. These results suggest that CQ-MAP can increase fibroblast cell viability and proliferation. In addition, PQ-MAP showed even higher cell viability and proliferation. Previous studies have used PQ formulations on skin and have described their effect on fibroblast and karyocytes, as well as the skin in general [41–43]. Therefore, the concentrations of PQ-MAP and CQ-MAP used in this study are biocompatible with fibroblast cells and could be used on the skin.

3.6. Stability study of MAPs

It has been suggested that MAPs have the potential to revolutionise how malaria is treated in developing countries by offering a simple and painless administration of antimalarial drugs in a sustained fashion [44]. Therefore, the stability of these MAPs during transportation and storage
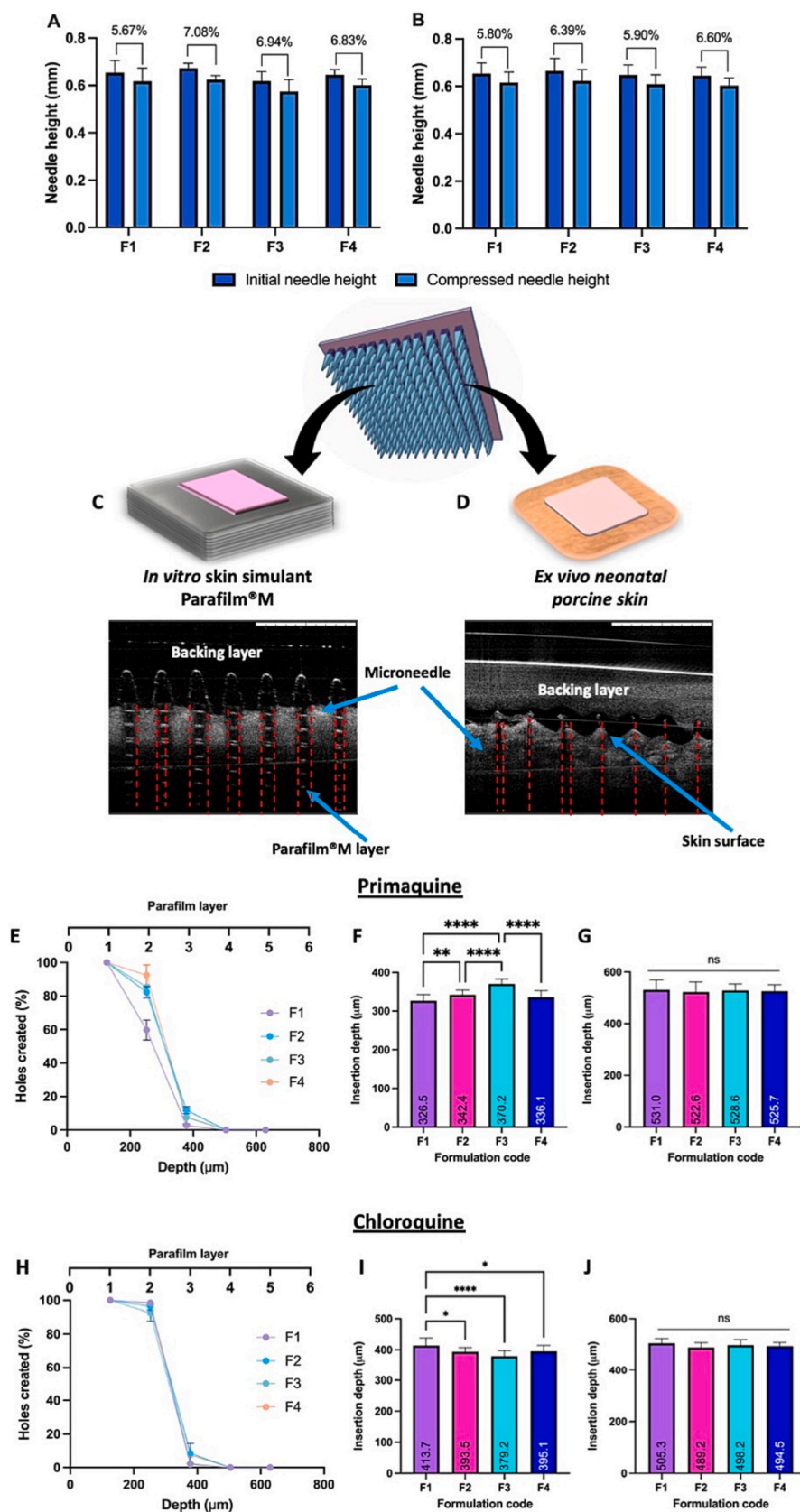
Fig. 6. The MAP height reduction for MAPs loaded with (A) PQ solid dispersion and (B) CQ solid dispersion was measured after applying a compressive force of 32 N (means + SD, $n = 20$). The OCT images of MAP insertion into (C) Parafilm®M and (D) *ex vivo* neonatal porcine skin. (E) The number of channels formed per layer of Parafilm® M was quantified following the application of MAPs loaded with (E) PQ and (H) CQ (means ± SD., $n = 3$). The depth at which PQ and CQ loaded MAPs penetrated into (F, I) Parafilm® M and (G, J) full thickness *ex vivo* neonatal porcine skin was measured (means + SD, n = 20).
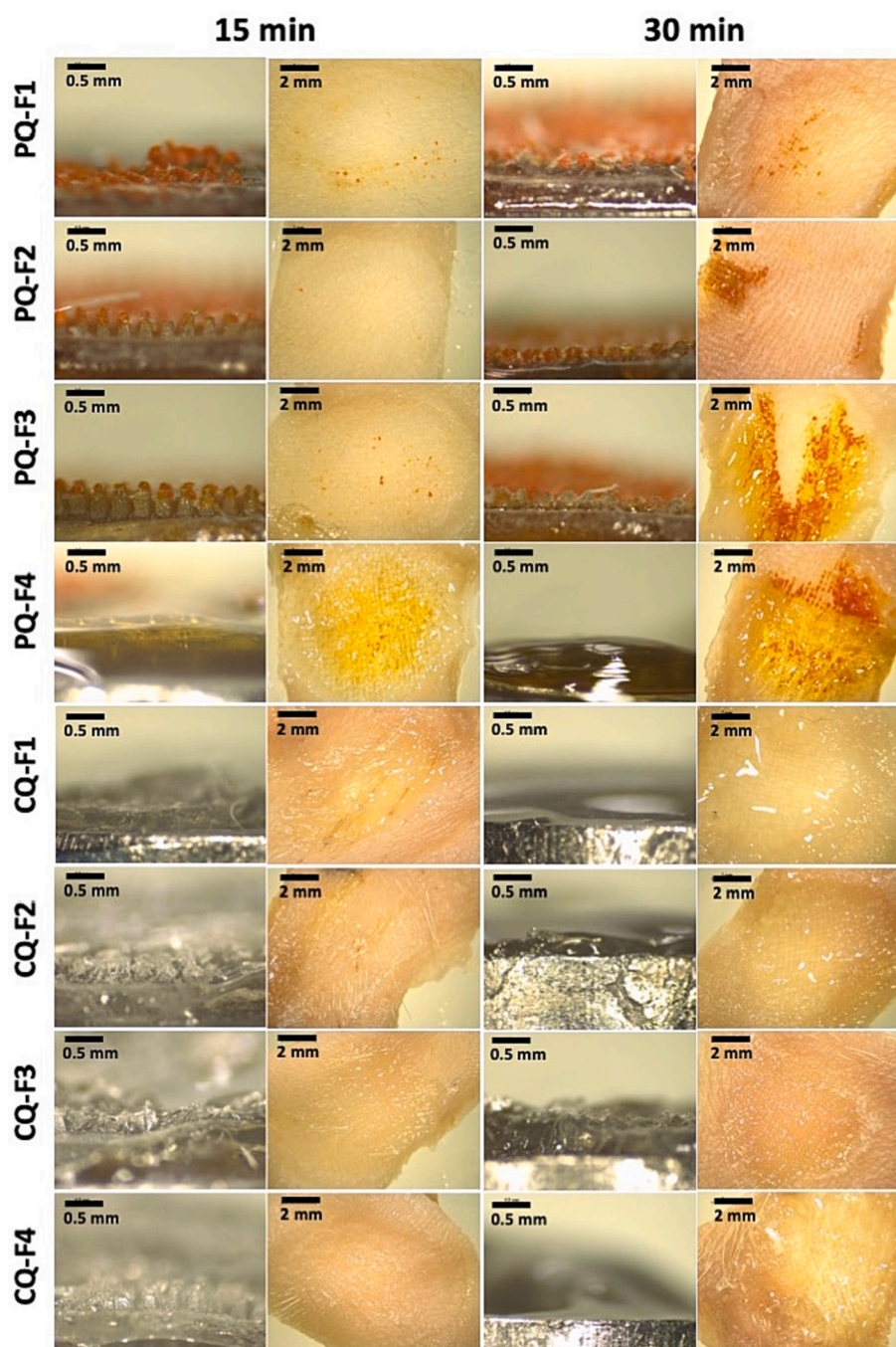
Fig. 7. *In-situ* skin dissolution PQ and CQ loaded MAPs at 15 mins and 30 min.

is of utmost importance, given the diverse temperature and humidity conditions in these regions. This is especially critical for dissolving MAPs, which are typically fabricated from water-soluble polymers that render them hygroscopic [32]. Exposure to the atmosphere may increase the propensity of the polymeric needle to trap moisture, leading to plasticisation along the needle length and weakening the overall mechanical properties of the MAP, resulting in poor insertion into the skin [45]. Therefore, this study also evaluated the stability of the MAPs during storage. The MAPs were stored under three different conditions: 5 °C and ambient humidity, 25 °C and 65% relative humidity, and 40 °C and 75% relative humidity for 30 and 90 days. In all cases, height reduction, drug content, and insertion depth were evaluated as indicators of formulation stability (Fig. 10). The results showed that there were no major differences in height reduction, drug content and

insertion depth were seen after 30 and 90 days for both CQ and PQ loaded dissolving MAPs.

The Food and Drug Administration (FDA) guidelines for drug products Q1A(R2) indicate that both thermal stability and sensitivity to moisture of pharmaceutical formulations should be evaluated, and storage conditions and lengths should be sufficient to cover the chain of storage, shipment, and subsequent use of the drug product [46]. In the present study, a total of three months was evaluated, which may cover the duration for the formulation to be manufactured, shipped, distributed, stored, and dispensed to the patient. This duration confirmed that the physical integrity of these MAPs (and their drug load) is maintained for at least 90 days. This preliminary stability study is promising, particularly as the MAPs were stored at 40 °C and 75% relative humidity, which typically represents a tropical atmosphere analogous to
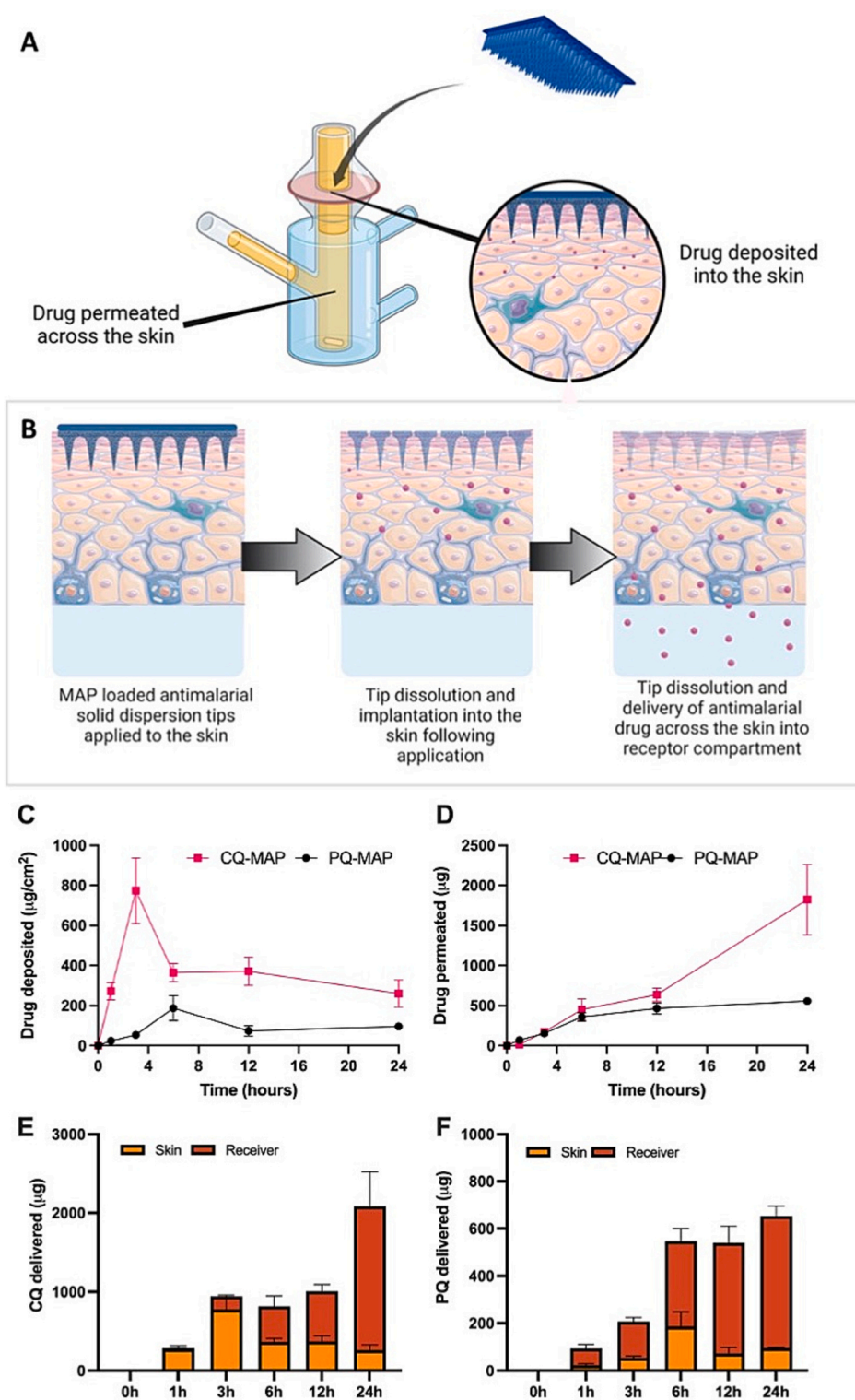
Fig. 8. (A) The schematic depicts the setup of the Franz cell, which is used to evaluate the deposition and permeation of drugs across porcine skin. (B) The diagram illustrates the proposed delivery mechanism of PQ and CQ across the skin. (C) Amount of drug extracted from skin layer at different time points following *in vitro* Franz cell diffusion study (means ± SD, *n* = 4). (D) Amount of drug delivered transdermally into the receiver compartment of Franz cells (means ± SD, n = 4). Drug distribution at different times after application (E) CQ and (F) PQ loaded dissolving MAP (means + SD, n = 4).

the countries where malaria is endemic. Nevertheless, further studies over a longer period of time should be conducted to validate the stability of dissolving MAPs. In addition, further studies evaluating the stability of these formulations before and after terminal sterilisation will also be essential to facilitate the translation of these systems into clinical practice.

3.7. Pharmacokinetic studies

After the *in vitro* permeation study, the dissolving MAPs loaded with PQ and CQ were chosen for further investigation *in vivo*. Upon removal of the MAPs after a 24-h application period, we observed complete dissolution of the needle layers, in line with the *in vitro* skin dissolution data. The pharmacokinetic profiles of both PQ and CQ following MAP and oral administration are shown in Fig. 11.

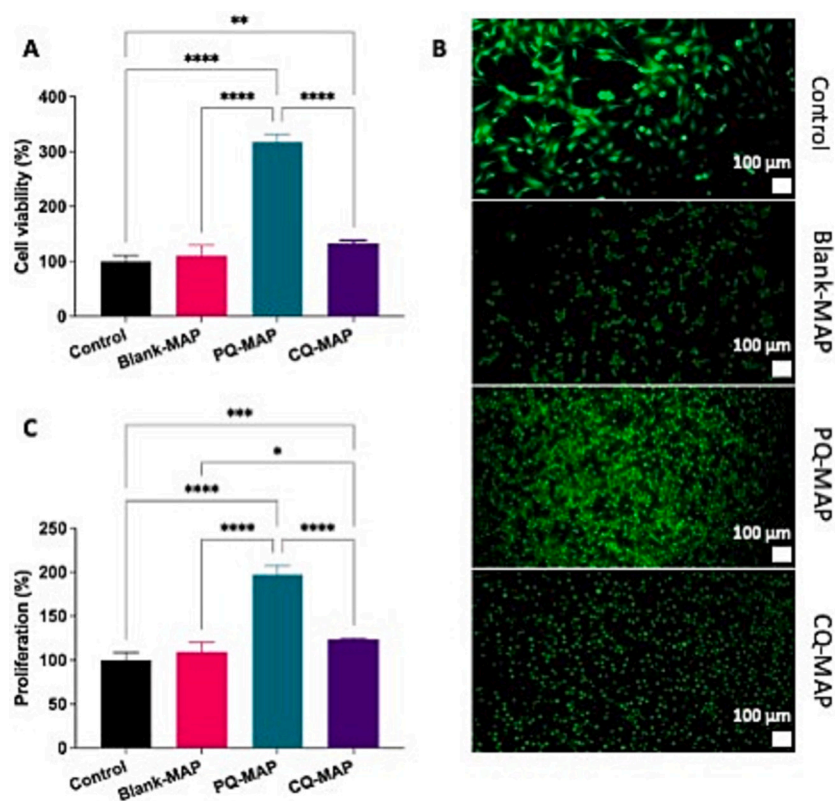For PQ, oral administration resulted in a rapid increase in plasma

Fig. 9. (A) Cell viability of fibroblast expressed as a percentage of viable cells when cultured on control cells, MAP-Blank, PQ-MAP and CQ-MAP (means + SD, $n = 6$). (B) Live/dead staining of fibroblast cells on control cells, MAP-Blank, PQ-MAP and CQ-MAP samples. Green represents for live cells. (C) PicoGreen assay results for total DNA content of fibroblast cells on Control cells, MAP-Blank, PQ-MAP and CQ-MAP (means + SD, n = 6). (For interpretation of the references to colour in this figure legend, the reader is referred to the web version of this article.)
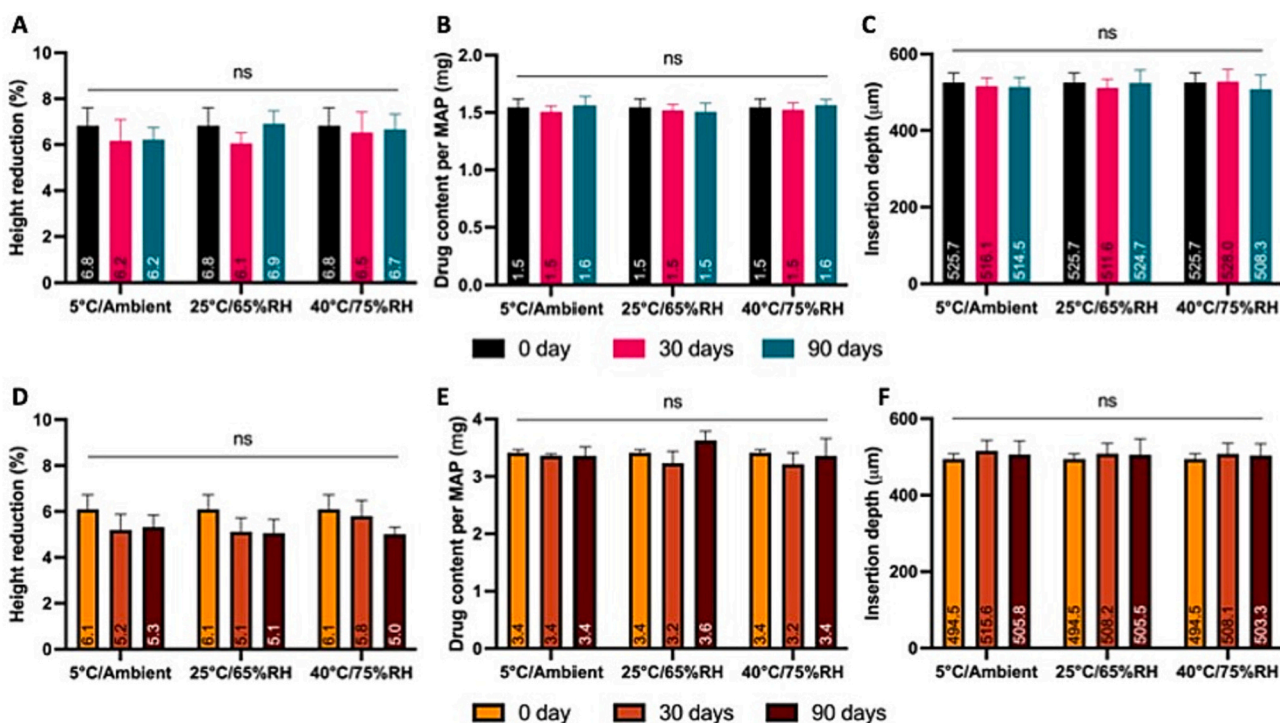

Fig. 10. Stability studies of (A-C) PQ-MAP and (D—F) CQ-MAP exposed to different temperature and humidity conditions and their evaluation of (A,D) drug content (means + SD, $n = 6$), (B,E) height reduction (means + SD, $n = 20$) and (C,F) insertion depth into *ex vivo* porcine skin (means + SD, n = 20).

concentration, reaching a C_{max} of $\approx$1600 ng/mL within 3 h, as shown in Table 3. However, when PQ was administered as a dissolving MAP, we observed a significant difference ($p < 0.05$) in T_{max}, which was 9.7 h. Additionally, the C_{max} for the MAP group was significantly lower than

that of the oral group. Furthermore, delivery of PQ *via* MAP resulted in a 20-fold lower AUC compared to oral administration. Nevertheless, the sustained drug delivery of PQ for up to 7 days by MAP could provide a simplified treatment regime, consisting of a single oral dose followed by
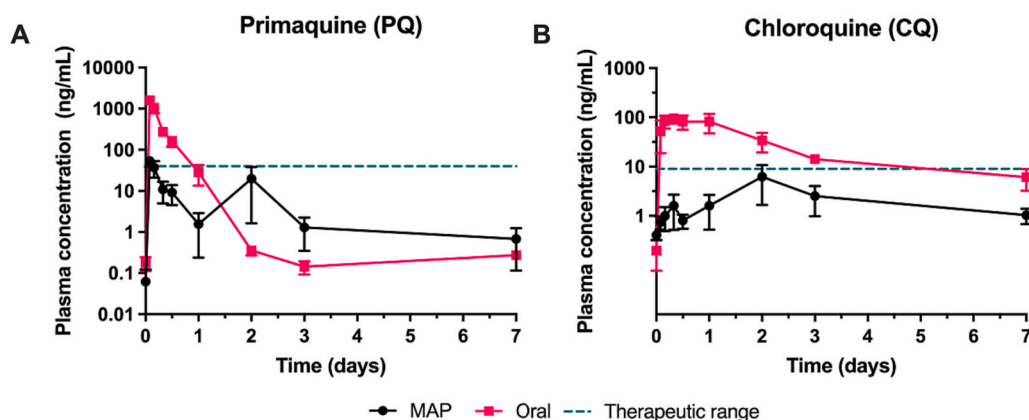
Fig. 11. Plasma levels of (A) PQ and (B) CQ were measured over time in rats treated with dissolving MAPs or administered through oral gavage. The results are presented as means $\pm$ SD ($n = 6$). In the dissolving MAP group, each rat received two MAPs, which is equal to 5.6 mg and 13.6 mg for PQ and CQ, respectively. The oral group received a dose of 30 mg/kg of PQ or CQ (equal to 13.5 mg of PQ or CQ) was administered.

Table 3
Pharmacokinetic parameters, AUC, C_{max}, T_{max}, half-life and mean residence time following dose administration. Data are expressed as mean $\pm$ SEM (n = 6).

Drug	Pharmacokinetic parameters	MAP treatment group	Oral treatment group
Primaquine	AUC (ng.hr/mL)	364 $\pm$ 40	8180 $\pm$ 1310
	C_{max} (ng/mL)	61.6 $\pm$ 16.9	1590 $\pm$ 320
	T_{max} (hr)	9.7 $\pm$ 7.7	3.0 $\pm$ 1.0
	$T_{1/2}$ (hr)	54.3 $\pm$ 25.7	49.5 $\pm$ 35.8
	MRT (hr)	64.8 $\pm$ 36.5	35.8 $\pm$ 2.2
	Dose administered (mg)	2.8	13.5
Choloroquine	AUC (ng.hr/mL)	755 $\pm$ 303	4900 $\pm$ 1200
	C_{max} (ng/mL)	6.5 $\pm$ 4.4	151 $\pm$ 19
	T_{max} (hr)	49.0 $\pm$ 25.2	10.0 $\pm$ 3.0
	$T_{1/2}$ (hr)	117 $\pm$ 54	30.0 $\pm$ 3.5
	MRT (hr)	192.4 $\pm$ 72.4	3.5 $\pm$ 4.8
	Dose administered (mg)	6.8	13.5

weekly patch application until complete parasitaemia eradication is achieved. Further study to investigate this formulation combination would be imperative to gauge the efficacy and feasibility of such a treatment strategy.

For CQ, oral administration resulted in a sharp rise in plasma concentration, reaching a C_{max} of ≈ 150 ng/mL within 10 h, as shown in Table 3. When CQ was administered as a dissolving MAP, we observed a significant change ($p < 0.05$) in T_{max}, which was prolonged from 10 h (for oral group) to 50 h. The C_{max} of the MAP group decreased to 6.5 ng/mL, and the AUC was six times lower than that of the oral group, potentially reducing the risk of hepatotoxicity. All liver specimens stained with H&E showed normal and healthy physiological features (Fig. 12), except for the group that received CQ *via* the oral route, which showed signs of intrahepatic cholestasis, a marker for hepatoxicity. In contrast, the delivery of CQ *via* dissolving MAP resulted in no noticeable signs of hepatoxicity [47,48]. Moreover, based on this proof-of-concept work, formulating the drugs into dissolving MAPs could potentially reduce the required administered dose. For instance, considering the therapeutic plasma levels of PQ ranging from 40 to 238 ng/mL [49], this study demonstrated that an adult patient with a body mass of 60 kg would require 77.83 mg of PQ transdermally over a 7-day period, while for oral administration, the patient would need to take 105 mg over the same duration. If we extrapolate these amounts to the MAP, the patch size required to achieve therapeutic levels in human clinical applications would be 42.25 cm^2. Similarly, for CQ, the therapeutic range for antiplasmodial activity is between 9 and 62 ng/mL [50]. An adult patient would require 189.03 mg of CQ *via* the transdermal route for a 7-day treatment period (equivalent to a 42.25 cm^2 patch), whereas oral administration would require 10,500 mg to achieve the therapeutic

range for curing *Plasmodium vivax*.

Accordingly, this study successfully demonstrated that by formulating the drugs into MAPs, the doses of antimalarial drugs can be reduced compared to oral tablets, as well as the frequency of administration. Although the patch size in this study is relatively large compared to marketed transdermal patches like Nicotinell patches, previous research has shown the successful application of large MAPs onto human skin [51]. Therefore, it is possible to design a proposed patch size to improve the delivery of antimalarial drugs.

Furthermore, delivering the antimalarial molecules *via* dissolving MAPs resulted in an increase in the mean residence time (MRT) of the drug in the body. This indicates that the drug remained exposed to the body for a longer duration, likely due to the dissolution of the needle layer from the patch upon administration. This process generates a micron-sized polymeric depot in the skin, which slowly releases the drug over several days [52]. The prolonged exposure to the drug, in a low yet sustained fashion, increases the likelihood of eradicating the parasite, avoid the parasite resistance, while reducing the risk of inducing unwanted side effects, such as hepatoxicity. Moreover, it is worth noting that we administered the same amount of CQ for both the MAP and oral groups. However, it can be observed that oral administration caused hepatoxicity, whereas this was not the case in the MAP group. This finding suggests that delivering the molecules *via* the transdermal route circumvents the potential first-pass metabolism and gastrointestinal side effects typically associated with oral delivery of antimalarial agents [53].

3.8. In vivo antimalarial activity in plasmodium berghei-infected mice

After evaluating the *ex vivo* and pharmacokinetic profiles of CQ-MAP and PQ-MAP, we proceeded to assess the efficacy of these formulations in eliminating *P. berghei* in infected mice. We conducted a study to evaluate the antimalarial activity of CQ-MAP, PQ-MAP, and a combination of CQ-MAP and PQ-MAP. The results showed that CQ-MAP and CQ-MAP+PQ-MAP were able to eliminate 99.2% of the parasites (Fig. 13). In comparison to the control group, which consisted of infected mice without any treatment, the group that received both CQ-MAP and PQ-MAP exhibited a significantly lower percentage of parasitemia ($p < 0.05$). However, there was no significant reduction in parasitemia observed in the group that received only PQ-MAP compared to the control group ($p > 0.05$). This result was expected, as PQ is typically used in combination with CQ to treat malaria caused by *P. vivax* [54]. PQ acts more slowly in reducing parasitemia and is primarily used to eliminate residual parasites and prevent resistance [55]. Furthermore, CQ-MAP showed a significant reduction in parasitemia compared to the control group ($p < 0.05$). This can be attributed to CQ's
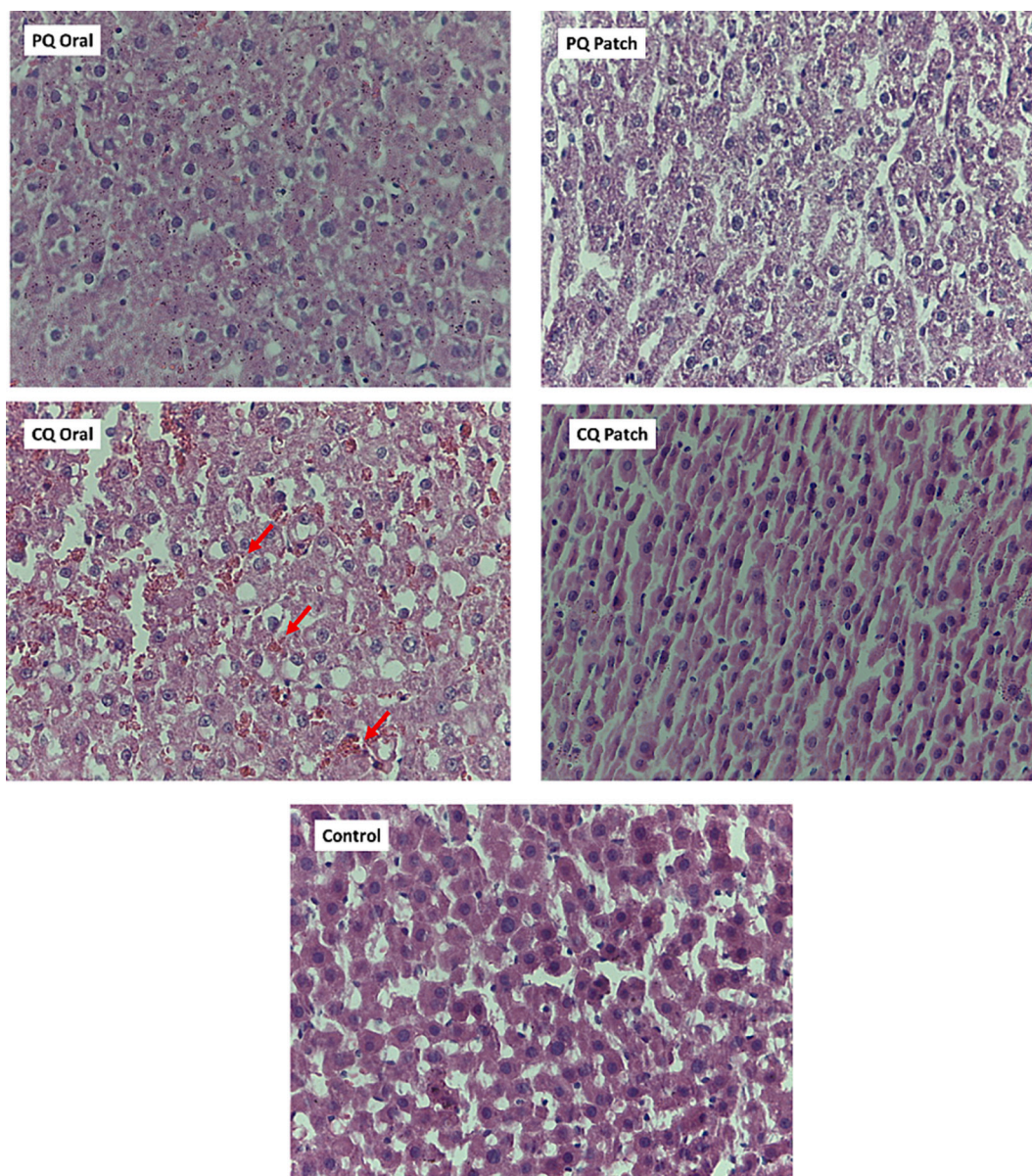
Fig. 12. Representative histological analysis of the liver of rats from treatment group. All images were viewed at x40 magnification.
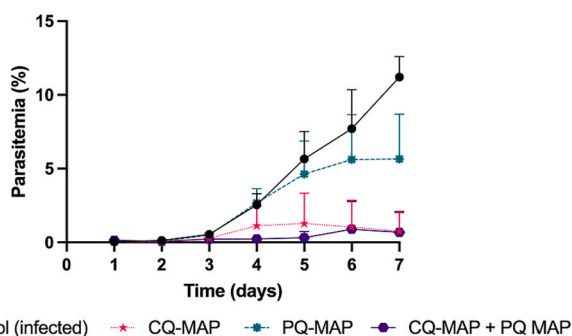

Fig. 13. Peripheral blood parasitaemia curves as a function of time to day 7 post-infection in groups of mice infected with murine parasite *P. berghei*. Control group: blank MAP (without drug). Treated group: PQ-MAP (1.4 mg), CQ-MAP (3.4 mg) and combination of PQ-MAP (1.4 mg) and CQ-MAP (3.4 mg) applied application (Mean + SD, $n = 7$).

rapid action in killing parasites, reducing parasitemia, and alleviating fever, which allows the patient to recover [56]. The combination of both drugs is crucial for achieving radical cure. The MAPs developed in this study demonstrated the ability to deliver a therapeutic amount of drugs into the bloodstream for up to seven days, resulting in parasite elimination and reduced hepatic toxicity, as confirmed by histological analysis (Fig. 12).

4. Conclusion

The results presented in this study demonstrate the successful development and characterisation of dissolving MAPs that are loaded with nano-sized solid dispersions of PQ and CQ in the tips. By incorporating the drugs as a solid dispersion, they exist in an amorphous state that facilitates rapid dissolution of the tip within 30 min upon application to the skin. Dermatokinetic studies revealed that most of the drug was delivered transdermally across the skin after 24 h. However, some drug was found to remain deposited in the skin, suggesting the potential for intradermal sustained release during malaria treatment. *In vivo* pharmacokinetic data in rats showed that these systems could provide

sustained transdermal delivery of PQ or CQ for over a week following a single 24-h patch application. Furthermore, efficacy studies in a murine model for malaria demonstrated that PQ-MAPs and CQ-MAPs were able to reduce parasitaemia up to 99.2% in treated animals. Overall, the current work highlights the potential of the engineered MAPs to offer a minimally invasive, needle-free drug delivery strategy for the treatment of malaria in low resource settings.

Funding

Ethical approval statement

NA.

Informed consent statement

NA.

CRediT authorship contribution statement

Qonita Kurnia Anjani: Visualization, Validation, Methodology, Investigation, Formal analysis, Data curation, Conceptualization, Writing – original draft, Writing – review & editing. **Fabiana Volpe-Zanutto:** Methodology, Investigation, Formal analysis, Data curation, Conceptualization, Validation, Writing – original draft, Writing – review & editing. **Khuriah Abdul Hamid:** Validation, Investigation, Formal analysis, Data curation, Methodology, Writing – original draft. **Akmal Hidayat Bin Sabri:** Methodology, Investigation, Writing – original draft. **Natalia Moreno-Castellano:** Visualization, Methodology, Investigation, Formal analysis, Data curation, Writing – original draft. **Xiomara Alexandra Gaitán:** Methodology, Investigation, Data curation. **Juliana Calit Paim:** Methodology, Investigation, Data curation. **Daniel Y. Bargier:** Supervision, Resources, Methodology, Investigation, Conceptualization, Writing – review & editing. **Ryan F. Donnelly:** Supervision, Resources, Project administration, Funding acquisition, Conceptualization, Writing – review & editing.

Declaration of Competing Interest

The authors declare no competing interest.

Data availability

The data is available from the corresponding author upon request.

References

[1] World malaria report 2022. https://www.who.int/teams/global-malaria-progra mme/reports/world-malaria-report-2022, 2022.

[2] K.E. Battle, J. Kevin Baird, The global burden of plasmodium vivax malaria is obscure and insidious, PLoS Med. 18 (2021) e1003799, https://doi.org/10.1371/ JOURNAL.PMED.1003799.

[3] K. Venugopal, F. Hentzschel, G. Valkiūnas, M. Marti, Plasmodium asexual growth and sexual development in the haematopoietic niche of the host, Nat. Rev. Microbiol. 18 (3) (2020) 177–189, https://doi.org/10.1038/s41579-019-0306-2.

[4] K. Thriemer, B. Ley, L. von Seidlein, Towards the elimination of plasmodium vivax malaria: implementing the radical cure, PLoS Med. 18 (2021) e1003494, https:// doi.org/10.1371/JOURNAL.PMED.1003494.

[5] K.E. Battle, T.C.D. Lucas, M. Nguyen, R.E. Howes, A.K. Nandi, K.A. Twohig, D. A. Pfeffer, E. Cameron, P.C. Rao, D. Casey, H.S. Gibson, J.A. Rozier, U. Dalrymple, S.H. Keddie, E.L. Collins, J.R. Harris, C.A. Guerra, M.P. Thorn, D. Bisanzio, N. Fullman, C.K. Huynh, X. Kulikoff, M.J. Kutz, A.D. Lopez, A.H. Mokdad, M. Naghavi, G. Nguyen, K.A. Shackelford, T. Vos, H. Wang, S.S. Lim, C.J.L. Murray, R.N. Price, J.K. Baird, D.L. Smith, S. Bhatt, D.J. Weiss, S.I. Hay, P.W. Gething, Mapping the global endemicity and clinical burden of plasmodium vivax, 2000–17: a spatial and temporal modelling study, Lancet 394 (2019) 332–343, https://doi. org/10.1016/S0140-6736(19)31096-7.

[6] J. Recht, E.A. Ashley, N.J. White, Use of primaquine and glucose-6-phosphate dehydrogenase testing: divergent policies and practices in malaria endemic countries, PLoS Negl. Trop. Dis. 12 (2018) e0006230, https://doi.org/ 10.1371/JOURNAL.PNTD.0006230.

[7] B.O. Carvalho, S.C.P. Lopes, P.A. Nogueira, P.P. Orlandi, D.Y. Bargieri, Y.C. Blanco, R. Mamoni, J.A. Leite, M.M. Rodrigues, I.S. Soares, T.R. Oliveira, G. Wunderlich, M.V.G. Lacerda, H.A. Del Portillo, M.O.G. Araújo, B. Russell, R. Suwanarusk, G. Snounou, L. Rénia, F.T.M. Costa, On the cytoadhesion of plasmodium vivax-infected erythrocytes, J. Infect. Dis. 202 (2010) 638–647, https://doi.org/ 10.1086/654815.

[8] E. Hempelmann, Hemozoin biocrystallization in plasmodium falciparum and the antimalarial activity of crystallization inhibitors, Parasitol. Res. 100 (2007) 671–676, https://doi.org/10.1007/s00436-006-0313-x.

[9] C.C. Biguetti, J.F.S. Junior, M.W. Fiedler, M.T. Marrelli, M. Brotto, The toxic effects of chloroquine and hydroxychloroquine on skeletal muscle: a systematic review and meta-analysis, Sci. Rep. 11 (2021) 6589, https://doi.org/10.1038/S41598- 021-86079-4.

[10] G. Camarda, P. Jirawatcharadech, R.S. Priestley, A. Saif, S. March, M.H.L. Wong, S. Leung, A.B. Miller, D.A. Baker, P. Alano, M.J.I. Paine, P.M. O'Neill, S.A. Ward, G.A. Biagini, Antimalarial activity of primaquine operates via a two-step biochemical relay, Nat. Commun. 10 (1) (2019) 1–9, https://doi.org/ 10.1038/s41467-019-11239-0.

[11] R.N. Price, N.M. Douglas, Expanding the use of Primaquine for the radical cure of plasmodium vivax, Clin. Infect. Dis. 67 (2018) 1008–1009, https://doi.org/ 10.1093/cid/ciy236.

[12] S. Srinivasan, D. Roy, T.E.J. Chavas, V. Vlaskin, D.K. Ho, A. Pottenger, C.L. M. LeGuyader, M. Maktabi, P. Strauch, C. Jackson, S.M. Flaherty, H. Lin, J. Zhang, B. Pybus, Q. Li, H.E. Huber, P.A. Burke, D. Wesche, R. Rochford, P.S. Stayton, Liver-targeted polymeric prodrugs of 8-aminoquinolines for malaria radical cure, J. Control. Release 331 (2021) 213–227, https://doi.org/10.1016/j. jconrel.2020.12.046.

[13] Joint Formulary Committee, BNF 82 (British National Formulary) September 2021, Pharmaceutical Press, 2021.

[14] C.S. Chu, N.J. White, Management of relapsing plasmodium vivax malaria, Expert Rev. Anti-Infect. Ther. 14 (2016) 885, https://doi.org/10.1080/ 14787210.2016.1220304.

[15] Q.K. Anjani, A.H. Bin Sabri, A.J. Hutton, Á. Cárcamo-Martínez, L.A.H. Wardoyo, A. Z. Mansoor, R.F. Donnelly, Microarray patches for managing infections at a global scale, J. Control. Release 359 (2023) 97–115, https://doi.org/10.1016/j. jconrel.2023.05.038.

[16] A.H. Sabri, Y. Kim, M. Marlow, D.J. Scurr, J. Segal, A.K. Banga, L. Kagan, J. Bong, Intradermal and transdermal drug delivery using microneedles – Fabrication, performance evaluation and application to lymphatic delivery, Adv. Drug Deliv. Rev. (2019), https://doi.org/10.1016/j.addr.2019.10.004.

[17] Q.K. Anjani, A. Hidayat, B. Sabri, N. Moreno-Castellanos, E. Utomo, Á. Cárcamo-Martínez, J. Domínguez-Robles, L. Ahmadi, H. Wardoyo, R.F. Donnelly, Soluplus®-based dissolving microarray patches loaded with colchicine: towards a minimally invasive treatment and management of gout, Biomater. Sci. (2022), https://doi. org/10.1039/D2BM01068B.

[18] Q. Kurnia, A. Hidayat, B. Sabri, J. Domínguez-robles, R.F. Donnelly, Metronidazole nanosuspension loaded dissolving microarray patches : an engineered composite pharmaceutical system for the treatment of skin and soft tissue infection, Biomater. Adv. 140 (2022), https://doi.org/10.1016/j.bioadv.2022.213073.

[19] Q.K. Anjani, A. Hidayat, B. Sabri, N. Moreno-castellanos, E. Utomo, Á. Cárcamo-martínez, J. Domínguez-robles, L. Ahmadi, H. Wardoyo, R.F. Donnelly, Soluplus®-based dissolving microarray patches loaded with colchicine: towards a minimally invasive treatment and management of gout, Biomater. Sci. (2022), https://doi. org/10.1039/d2bm01068b.

[20] Q.K. Anjani, A.H. Bin Sabri, K.A. Hamid, N. Moreno-Castellanos, H. Li, R. F. Donnelly, Tip loaded cyclodextrin-carvedilol complexes microarray patches, Carbohydr. Polym. 320 (2023) 121194, https://doi.org/10.1016/j. carbpol.2023.121194.

[21] R.F. Donnelly, M.T.C. McCrudden, A.Z. Alkilani, E. Larrañeta, E. McAlister, A. J. Courtenay, M.C. Kearney, T.R. Raj Singh, H.O. McCarthy, V.L. Kett, E. Caffarel-Salvador, S. Al-Zahrani, A.D. Woolfson, Hydrogel-forming microneedles prepared from "super swelling" polymers combined with lyophilised wafers for transdermal drug delivery, PLoS One 9 (2014), https://doi.org/10.1371/journal. pone.0111547.

[22] R.F. Donnelly, T.R.R. Singh, M.J. Garland, K. Migalska, R. Majithiya, C. M. McCrudden, P.L. Kole, T.M.T. Mahmood, H.O. McCarthy, A.D. Woolfson, Hydrogel-forming microneedle arrays for enhanced transdermal drug delivery, Adv. Funct. Mater. 22 (2012) 4879–4890, https://doi.org/10.1002/ adfm.201200864.

[23] Q.K. Anjani, A.D. Permana, Á. Cárcamo-Martínez, J. Domínguez-Robles, I. A. Tekko, E. Larrañeta, L.K. Vora, D. Ramadon, R.F. Donnelly, Versatility of hydrogel-forming microneedles in in vitro transdermal delivery of tuberculosis drugs, Eur. J. Pharm. Biopharm. 158 (2021) 294–312, https://doi.org/10.1016/j. ejpb.2020.12.003.

[24] A.H. Bin Sabri, Q.K. Anjani, E. Utomo, A. Ripolin, R.F. Donnelly, Development and characterization of a dry reservoir-hydrogel-forming microneedles composite for minimally invasive delivery of cefazolin, Int. J. Pharm. 617 (2022), 121593, https://doi.org/10.1016/J.IJPHARM.2022.121593.

[25] Q.K. Anjani, A.H. Bin Sabri, J. Domínguez-Robles, N. Moreno-Castellanos, E. Utomo, L.A.H. Wardoyo, E. Larrañeta, R.F. Donnelly, Metronidazole nanosuspension loaded dissolving microarray patches: an engineered composite

pharmaceutical system for the treatment of skin and soft tissue infection, Biomater. Adv. 140 (2022), 213073, https://doi.org/10.1016/J.BIOADV.2022.213073.

[26] D.A. Baker, L.B. Stewart, J.M. Large, P.W. Bowyer, K.H. Ansell, M.B. Jiménez-Díaz, M. El Bakkouri, K. Birchall, K.J. Dechering, N.S. Bouloc, P.J. Coombs, D. Whalley, D.J. Harding, E. Smiljanic-Hurley, M.C. Wheldon, E.M. Walker, J.T. Dessens, M. J. Lafuente, L.M. Sanz, F.J. Gamo, S.B. Ferrer, R. Hui, T. Bousema, I. Angulo-Barturén, A.T. Merritt, S.L. Croft, W.E. Gutteridge, C.A. Kettleborough, S. A. Osborne, A potent series targeting the malarial cGMP-dependent protein kinase clears infection and blocks transmission, Nat. Commun. 8 (2017) 1–9, https://doi.org/10.1038/s41467-017-00572-x.

[27] F. Volpe-Zanutto, L. Tiburcio, A. Dian, M. Kirkby, A.J. Paredes, L.K. Vora, A. P. Bonfanti, I. Charlie-silva, C. Raposo, M.C. Figueiredo, I.M.O. Sousa, A. Brisibe, R. F. Donnelly, M. Ann, F. Trindade, Artemether and Lumefantrine Dissolving Microneedle Patches with Improved Pharmacokinetic Performance and Antimalarial Efficacy in Mice Infected with Plasmodium Yoelii 333, 2021, pp. 298–315, https://doi.org/10.1016/j.jconrel.2021.03.036.

[28] Q.K. Anjani, Á. Cárcamo-Martínez, L.A.H. Wardoyo, N. Moreno-Castellanos, A. H. Bin Sabri, E. Larrañeta, R.F. Donnelly, MAP-box: a novel, low-cost and easy-to-fabricate 3D-printed box for the storage and transportation of dissolving microneedle array patches, Drug Deliv. Transl. Res. (2023), https://doi.org/10.1007/s13346-023-01393-w.

[29] M. Danaei, M. Dehghankhold, S. Ataei, F. Hasanzadeh Davarani, R. Javanmard, A. Dokhani, S. Khorasani, M.R. Mozafari, Impact of particle size and polydispersity index on the clinical applications of Lipidic Nanocarrier systems, Pharmaceutics. 10 (2018), https://doi.org/10.3390/PHARMACEUTICS10020057.

[30] S. Bhattacharjee, DLS and zeta potential - what they are and what they are not? J. Control. Release 235 (2016) 337–351, https://doi.org/10.1016/j.jconrel.2016.06.017.

[31] Q. Kurnia, A. Hidayat, B. Sabri, J. Domínguez-robles, R.F. Donnelly, Metronidazole nanosuspension loaded dissolving microarray patches : an engineered composite pharmaceutical system for the treatment of skin and soft tissue infection, Biomater. Adv. 140 (2022), https://doi.org/10.1016/j.bioadv.2022.213073.

[32] Q.K. Anjani, A. Hidayat, B. Sabri, N. Moreno-castellanos, E. Utomo, Á. Cárcamo-martínez, J. Domínguez-robles, L. Ahmadi, H. Wardoyo, R.F. Donnelly, Soluplus®-based dissolving microarray patches loaded with colchicine: towards a minimally invasive treatment and management of gout, Biomater. Sci. (2022), https://doi.org/10.1039/d2bm01068b.

[33] P. González-Vázquez, E. Larrañeta, M.T.C. McCrudden, C. Jarrahian, A. Rein-Weston, M. Quintanar-Solares, D. Zehrung, H. McCarthy, A.J. Courtenay, R. F. Donnelly, Transdermal delivery of gentamicin using dissolving microneedle arrays for potential treatment of neonatal sepsis, J. Control. Release 265 (2017) 30–40, https://doi.org/10.1016/j.jconrel.2017.07.032.

[34] A.D. Permana, A.J. Paredes, F. Volpe-Zanutto, Q.K. Anjani, E. Utomo, R. F. Donnelly, Dissolving microneedle-mediated dermal delivery of itraconazole nanocrystals for improved treatment of cutaneous candidiasis, Eur. J. Pharm. Biopharm. 154 (2020) 50–61, https://doi.org/10.1016/j.ejpb.2020.06.025.

[35] A.H. Sabri, Z. Cater, P. Gurnani, J. Ogilvie, J. Segal, D.J. Scurr, M. Marlow, Intradermal delivery of imiquimod using polymeric microneedles for basal cell carcinoma, Int. J. Pharm. 589 (2020), 119808, https://doi.org/10.1016/j.ijpharm.2020.119808.

[36] Q.K. Anjani, A.H. Bin Sabri, E. Utomo, J. Domínguez-Robles, R.F. Donnelly, Elucidating the Impact of Surfactants on the Performance of Dissolving Microneedle Array Patches, Mol Pharm, 2022, https://doi.org/10.1021/acs.molpharmaceut.1c00988.

[37] Assessing the Technical and Programmatic Feasibility of a Microarray Patch for Intradermal Delivery of Primaquine to Treat *P. vivax* | PATH. https://www.path.org/resources/assessing-the-technical-and-programmatic-feasibility-of-a-microarray-patch-for-intradermal-delivery-of-primaquine-to-treat-p-vivax/, 2017.

[38] F. Volpe-Zanutto, L.T. Ferreira, A.D. Permana, M. Kirkby, A.J. Paredes, L.K. Vora, A.P. Bonfanti, I. Charlie-Silva, C. Raposo, M.C. Figueiredo, I.M.O. Sousa, A. Brisibe, F.T.M. Costa, R.F. Donnelly, M.A. Foglio, Artemether and lumefantrine dissolving microneedle patches with improved pharmacokinetic performance and antimalarial efficacy in mice infected with plasmodium yoelii, J. Control. Release 333 (2021) 298–315, https://doi.org/10.1016/j.jconrel.2021.03.036.

[39] C.B.E. Braga, A.C. Martins, A.D.E. Cayotopa, W.W. Klein, A.R. Schlosser, A.F. Da Silva, M.N. De Souza, B.W.B. Andrade, J.A. Filgueira-Júnior, W. De Jesus Pinto, M. Da Silva-Nunes, Side effects of chloroquine and primaquine and symptom reduction in malaria endemic area (Mâncio Lima, Acre, Brazil), Interdiscip. Perspect. Infect. Dis. 2015 (2015), https://doi.org/10.1155/2015/346853.

[40] S.C. Tang, J.L. Ko, C. Te Lu, P.Y. Leong, C.C. Ou, C.T. Hsu, Y.P. Hsiao, Chloroquine alleviates the heat-induced to injure via autophagy and apoptosis mechanisms in

skin cell and mouse models, PLoS One 17 (2022), https://doi.org/10.1371/JOURNAL.PONE.0272797.

[41] C.W. Jeans, C.M. Heard, A therapeutic dose of primaquine can be delivered across excised human skin from simple transdermal patches, Int. J. Pharm. 189 (1999) 1–6, https://doi.org/10.1016/S0378-5173(99)00215-X.

[42] C.M. Heard, B.V. Monk, A.J. Modley, Binding of primaquine to epidermal membranes and keratin, Int. J. Pharm. 257 (2003) 237–244, https://doi.org/10.1016/S0378-5173(03)00140-6.

[43] K.K. Nishi, A. Jayakrishnan, Self-gelling primaquine-gum Arabic conjugate: an injectable controlled delivery system for primaquine, Biomacromolecules. 8 (2007) 84–90, https://doi.org/10.1021/BM060612X/ASSET/IMAGES/LARGE/BM060612XF00009.JPEG.

[44] A.J. Paredes, I.K. Ramöller, P.E. McKenna, M.T.A. Abbate, F. Volpe-Zanutto, L. K. Vora, M. Kilbourne-Brook, C. Jarrahian, K. Moffatt, C. Zhang, I.A. Tekko, R. F. Donnelly, Microarray patches: breaking down the barriers to contraceptive care and HIV prevention for women across the globe, Adv. Drug Deliv. Rev. 173 (2021) 331–348, https://doi.org/10.1016/j.addr.2021.04.002.

[45] E. McAlister, M.C. Kearney, E.L. Martin, R.F. Donnelly, From the laboratory to the end-user: a primary packaging study for microneedle patches containing amoxicillin sodium, Drug Deliv. Transl. Res. (2021) 1–17, https://doi.org/10.1007/s13346-020-00883-5.

[46] Q1A(R2) Stability Testing of New Drug Substances and Products | FDA. https://www.fda.gov/regulatory-information/search-fda-guidance-documents/q1ar2-stability-testing-new-drug-substances-and-products, 2003.

[47] L. Pari, D.R. Amali, Protective role of tetrahydrocurcumin (THC) an active principle of turmeric on chloroquine induced hepatotoxicity in rats, J. Pharm. Pharm. Sci. 8 (2005) 115–123.

[48] R. Wielgo-Polanin, L. Lagarce, E. Gautron, B. Diquet, P. Lainé-Cessac, Hepatotoxicity associated with the use of a fixed combination of chloroquine and proguanil, Int. J. Antimicrob. Agents 26 (2005) 176–178, https://doi.org/10.1016/j.ijantimicag.2005.04.019.

[49] A.G.N.C. Mello, M.V.D.F. Vieira, L.W.P. de Sena, T.P. da Paixão, A.C.G. Pinto, D. P. de A Grisólia, M.T. Silva, J.L.F. Vieira, Levels of primaquine and carboxyprimaquine in patients with malaria *vivax* from the Brazilian Amazon basin, Rev. Inst. Med. Trop. Sao Paulo 60 (2018), e66, https://doi.org/10.1590/S1678-9946201860066.

[50] O. Walker, A. Dawodu, A. Adeyokunnu, L. Salako, G. Alvan, Plasma chloroquine and desethylchloroquine concentrations in children during and after chloroquine treatment for malaria, Br. J. Clin. Pharmacol. 16 (1983) 701–705, https://doi.org/10.1111/J.1365-2125.1983.TB02244.X.

[51] A.H. Sabri, Z. Cater, P. Gurnani, J. Ogilvie, J. Segal, D.J. Scurr, M. Marlow, Intradermal delivery of imiquimod using polymeric microneedles for basal cell carcinoma, Int. J. Pharm. 589 (2020), 119808, https://doi.org/10.1016/j.ijpharm.2020.119808.

[52] C.B.E. Braga, A.C. Martins, A.D.E. Cayotopa, W.W. Klein, A.R. Schlosser, A.F. Da Silva, M.N. De Souza, B.W.B. Andrade, J.A. Filgueira-Júnior, W. De Jesus Pinto, M. Da Silva-Nunes, Side effects of chloroquine and primaquine and symptom reduction in malaria endemic area (Mâncio lima, Acre, Brazil), Interdiscip. Perspect. Infect. Dis. 2015 (2015), https://doi.org/10.1155/2015/346853.

[53] J. Recht, A.M. Siqueira, W.M. Monteiro, S.M. Herrera, S. Herrera, M.V.G. Lacerda, Malaria in Brazil, Colombia, Peru and Venezuela: Current challenges in malaria control and elimination, Malar. J. 16 (2017) 1–18, https://doi.org/10.1186/s12936-017-1925-6.

[54] R.J. Commons, J.A. Simpson, K. Thriemer, G.S. Humphreys, T. Abreha, S.G. Alemu, A. Añez, N.M. Anstey, G.R. Awab, J.K. Baird, T.E. Barber, I. Borghini-Fuhrer, C. S. Chu, U. D'Alessandro, P. Dahal, A. Daher, P.J. de Vries, A. Erhart, M.S.M. Gomes, L. Gonzalez-Ceron, M.J. Grigg, A. Heidari, J. Hwang, P.A. Kager, T. Ketema, W. A. Khan, M.V.G. Lacerda, T. Leslie, B. Ley, K. Lidia, W.M. Monteiro, F. Nosten, D. B. Pereira, G.T. Phan, A.P. Phyo, M. Rowland, K. Saravu, C.H. Sibley, A. M. Siqueira, K. Stepniewska, I. Sutanto, W.R.J. Taylor, G. Thwaites, B.Q. Tran, H. T. Tran, N. Valecha, J.L.F. Vieira, S. Wangchuk, T. William, C.J. Woodrow, L. Zuluaga-Idarraga, P.J. Guerin, N.J. White, R.N. Price, The effect of chloroquine dose and primaquine on plasmodium vivax recurrence: a WorldWide antimalarial resistance network systematic review and individual patient pooled meta-analysis, Lancet Infect. Dis. 18 (2018) 1025–1034, https://doi.org/10.1016/S1473-3099(18)30348-7.

[55] A. Miatmoko, I. Nurjannah, N.F. Nehru, N. Rosita, E. Hendradi, R. Sari, J. Ekowati, Interactions of primaquine and chloroquine with PEGylated phosphatidylcholine liposomes, Sci. Rep. 11 (2021) 1–12, https://doi.org/10.1038/s41598-021-91866-0.